JCI The Journal of Clinical Investigation

TRIM56 protects against non-alcoholic fatty liver disease via promoting the degradation of fatty acid synthase

Suowen Xu, … , Yan-Xiao Ji, Jianping Weng

J Clin Invest. 2024. https://doi.org/10.1172/JCI166149.

Research In-Press Preview Hepatology

Graphical abstract

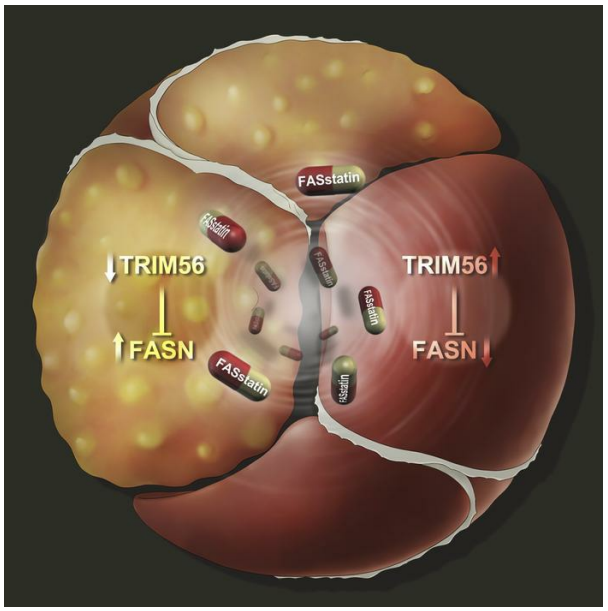

TRIM56 protects against non-alcoholic fatty liver disease via promoting the degradation of fatty acid synthase

Suowen Xu[1#], Xiumei Wu[2,3#], Sichen Wang[4#], Mengyun Xu[1], Tingyu Fang[1], Xiaoxuan Ma[1], Meijie Chen[1], Jiajun Fu[5], Juan Guo[6], Song Tian[4], Tian Tian[6], Xu Cheng[5], Hailong Yang[5], Junjie Zhou[5], Zhenya Wang[8], Yanjun Yin[9], Wen Xu[3], Fen Xu[3], Jinua Yan[3], Zhihua Wang[1], Sihui Luo[1], Xiao-Jing Zhang[4], Yan-Xiao Ji[4], Jianping Weng[1,3,*]

Affiliations:

[1]Department of Endocrinology, Institute of Endocrine and Metabolic Diseases, The First Affiliated Hospital of USTC, Division of Life Sciences and Medicine, Clinical Research Hospital of Chinese Academy of Sciences (Hefei), University of Science and Technology of China; Hefei, 230001, China

[2]Department of Endocrinology, Guangdong Geriatrics Institute, Guangdong Academy of Medical Sciences, Guangdong Provincial People's Hospital

[3]Department of Endocrinology and Metabolism, The Third Affiliated Hospital of Sun Yat-sen University; Guangzhou, China.

[4]School of Basic Medical Sciences, Wuhan University; Wuhan 430071, China.

[5]State Key Laboratory of New Targets Discovery and Drug Development for Major Diseases; Gannan Innovation and Translational Medicine Research Institute; Gannan Medical University; Ganzhou, China.

[6]School of Medical Information Engineering, Gannan Medical University, Gannan Medical University, Ganzhou, China.

[7]College of Life Sciences, Wuhan University; Wuhan, China

[8]Department of Cardiology, Renmin Hospital of Wuhan University; Wuhan, China.

[9]School of Pharmacy, Bengbu Medical College, Bengbu, 233000, China.

Short title: TRIM56 in NAFLD/NASH

Declaration of interests: The authors have declared that no conflict of interest exists.

#These authors contributed equally to this work

*Corresponding author.

Jianping Weng, MD

The First Affiliated Hospital of USTC,

Division of Life Sciences and Medicine,

University of Science and Technology of China;

Hefei, 230001, China

Phone: +86-551-63602683

Email: wengjp@ustc.edu.cn;

Abstract

Nonalcoholic liver disease (NAFLD) encompasses a disease continuum from simple steatosis, to non-alcoholic steatohepatitis (NASH). However, there are currently no approved pharmacotherapies for NAFLD although several drugs are in advanced stages of clinical development. Because of the complex pathophysiology and heterogeneity of NALFD, identification of potential therapeutic targets is clinically important. Here, we demonstrated that TRIM56 protein abundance is markedly downregulated in the livers of individuals with NAFLD and mice fed a high-fat diet. Hepatocyte-specific ablation of TRIM56 exacerbated the progression of NAFLD, while hepatic TRIM56 overexpression suppressed it. Integrative analyses of interactomic and transcriptomic profiling revealed a pivotal role of TRIM56 in lipid metabolism and identified lipogenesis factor FASN as a direct binding partner of TRIM56. TRIM56 directly interacts with FASN and triggers its K48-linked ubiquitination-dependent degradation. Finally, by using AI-based virtual screening, we discovered an orally bioavailable small-molecule inhibitor of FASN (named FASstatin) which potentiates TRIM56-mediated FASN ubiquitination. Therapeutic administration of FASstatin improved NAFLD and NASH pathologies in mice with optimal safety, tolerability and pharmacokinetic profile. Our findings provide the proof-of-concept that targeting the TRIM56/FASN axis in hepatocytes may offer potential therapeutic avenues to treat NAFLD.

Keywords: TRIM56, NAFLD, NASH, FASstatin, FASN

Introduction

Non-alcoholic fatty liver disease (NAFLD) is the most prevalent metabolic dysfunction-associated steatotic liver disease due to the global obesity epidemic (1-3). The complex interplay between genetic, epigenetic, metabolic, dietary and environmental factors underlies the mechanistic basis of NAFLD (4). NAFLD remains silent and asymptomatic even until progressing into nonalcoholic steatohepatitis (NASH), the advanced stage of NAFLD featured by hepatic steatosis, inflammation, fibrosis and liver damage, which might ultimately lead to life-threatening sequelae, including cirrhosis, hepatocellular carcinoma (HCC) and liver failure (5, 6). Currently, only bariatric-metabolic surgery, lifestyle interventions and dietary alterations are recommended for the treatment of NAFLD (7). Although there are >70 candidate drugs in the therapeutic pipeline, no disease-modifying agents have been approved as effective pharmacotherapies against NAFLD/NASH (5), highlighting the urgent medical need to identify target-based medical therapy for NAFLD/NASH.

Metabolic perturbations in NAFLD/NASH are driven by fatty acid synthesis pathways (8, 9). Increased fatty acid synthesis driven by nutrient surplus leads to lipotoxicity and metabolic stress, and resultant body weight gain and cardiometabolic risk factors associated with NAFLD/NASH (10). The ubiquitin–proteasome pathway is crucial for protein degradation and thus controls protein turnover and could potentially regulate metabolic surplus-induced metabolic dysfunction. The extent of ubiquitination is determined by the concerted actions of ubiquitinases and deubiquitinases. In this regard, TRIM (tripartite motif)-containing proteins comprise a large family of RING domain-containing E3 ubiquitin ligases that regulate inflammation, immunity, fibrosis and cancer (11-14). However, only a few members of TRIM family have been investigated in the context of metabolic disorders thus far.

In the present study, with an aim to discovering essential molecular factor(s) controlling NAFLD pathogenesis, we established a multilayer screening approach, ranging from transcriptomics analysis of human and mouse NAFLD samples to siRNA library screening followed by functional evaluation. We discovered that TRIM family of proteins are a conserved family of proteins that play important roles in hepatic steatosis and NAFLD development. Among TRIM family members, TRIM56 was identified as an endogenous negative regulator of hepatic lipid accumulation by directly interacting with FASN and promotes its degradation. More importantly, by integrating artificial intelligence (AI)-assisted drug discovery, we identified a FASN inhibitor-FASstatin, which can promote TRIM56-mediated FASN protein degradation and suppress NAFLD in mice with good efficacy and safety profile. The present study extends the recognized role of TRIM56 in antiviral innate immunity (15) and offers a potential pharmaceutical intervention strategy of NAFLD by targeting TRIM56-FASN axis.

Results

Identification of TRIM56 as a key regulator of NAFLD

To elucidate potential therapeutic targets of NAFLD, we first performed an integrative analysis in published NAFLD datasets in mouse and human. In total, 4 human NAFLD published datasets and 11 mouse NAFLD datasets were included for analysis. The intersection of gene sets enriched in NAFLD group in all human NAFLD databases and gene sets enriched in HFD group in all mouse NAFLD databases was considered as candidate protein families. Our analysis pinpoints TRIM protein family as a conserved family of with altered gene expression in mouse and human NAFLD (Figure 1A-1D). To date, the impact of the TRIM family of E3 ligases on hepatocyte lipid metabolism remains largely unexplored. Till now, more than 70 TRIM family

members have been identified. In order to further reveal the key TRIM family member in hepatic steatosis, we performed an unbiased siRNA library screening of 73 TRIM family members using Nile Red-based lipid accumulation in palmitic acid/oleic acid (PO)-challenged hepatocytes as the functional readout. We transfected hepatocytes with individual siRNAs at 50 nM for 48 h in the presence of PO exposure before Nile Red staining by high-content imaging. Our screening data revealed that TRIM56 is a prominent suppressor of lipid accumulation compared with other TRIM members (Figure 1E-1F). Validation studies support that TRIM56 depletion by siRNA further aggravates PO-induced lipid accumulation (Figure S1 and Figure 1G).

We next explored the possibility whether or not hepatocyte-derived TRIM56 plays an important role in hepatic steatosis and NAFLD pathogenesis. Since lipotoxicity driven by excessive free fatty acid accumulation is a key driver of NAFLD, we first evaluated protein expression of TRIM56 upon exposure to PO in primary mouse hepatocytes, as well as to LPS in Kupffer cells and TGF-β1 in hepatic stellate cells (HSCs). We observed that downregulation of TRIM56 protein occurred only in PO-challenged mouse and human hepatocytes (Figure 1H-1I), instead of LPS-challenged Kupffer cells (Figure 1J) or TGF-β1-challenged HSCs (Figure 1K). We then examined the effect of NAFLD on TRIM56 gene and protein expression in liver tissues. We observed that the protein expression level, rather than gene expression level of TRIM56 was markedly downregulated in mice fed a high fat diet (HFD) as well as in individuals with NAFLD, as revealed by western blot analysis and immunofluorescent staining (Figure 1L-O and Figure S2A-S2C). Further analysis revealed that PO challenge increased TRIM56 ubiquitination and TRIM56 underwent self-ubiquitination as E3-ligase catalytically inactive mutant of TRIM56 failed to cause ubiquitination of TRIM56 (Figure S2D-S2E). These data highlight a potential role

of hepatocyte-derived TRIM56 in the progression of NAFLD. Altogether, these results indicate that the downregulation of TRIM56 is associated with NAFLD.

TRIM56 blocks hepatocyte lipid accumulation

Based on the observations that TRIM56 protein expression was decreased in NAFLD mice, human subjects and PO-challenged hepatocytes, we hypothesized that TRIM56 could potentially confer protection against NAFLD. To determine the precise role of *Trim56* in lipid accumulation in vitro, we applied Nile Red staining as a proxy for cytosolic lipid droplet accumulation. We first explored the possibility that TRIM56 gain-of-function by adenovirus-mediated overexpression could attenuate lipid accumulation in hepatocytes. We observed that *Trim56* overexpression dampens lipid droplet accumulation and mitigates intracellular TG accumulation in hepatocytes stimulated with PO (Figure 2A-2C). Consistently, the expression of genes associated with fatty acid metabolism was attenuated by *Trim56* overexpression (Figure 2D). In contrast, *Trim56*-deficient hepatocytes accumulated more lipid droplets upon PO stimulation with paralleled increase in intracellular TG measurements (Figure 2E-2G). To dissect the role of *Trim56* in lipid metabolism, we performed RNA-sequencing analysis on wild-type (WT) and *Trim56*-deficient hepatocytes upon exposure to PO. Our transcriptomic profiling data revealed that TRIM56 ablation led to the upregulation of pathways enriched in fatty acid biosynthesis, lipid metabolism and steroid metabolism (Figure 2H-2K). Collectively, these results suggest a potential role for TRIM56 to protect against NAFLD.

Hepatocyte TRIM56 protects against HFD-induced hepatic steatosis

To investigate the impact of TRIM56 in hepatocytes on NAFLD pathogenesis in vivo, we generated hepatocyte-specific *Trim56* knockout mice by AAV8-*Trim56*-sgRNA-TBG-cre injection. Significantly decreased TRIM56 protein level was observed in *Trim56* conditional knockout mouse (*Trim56*-HepKO) livers (Figure 3A). We then evaluated the impact of hepatocyte-specific *Trim56* ablation on HFD-accelerated NAFLD development in mice. We observed that liver weight and hepatic TG level were increased in *Trim56*-HepKO mice (Figure 3B-3C). Similarly, increased hepatic steatosis and lipid droplet accumulation were observed in *Trim56*-HepKO mice (Figure 3D). In addition, circulating levels of total cholesterol (TC), ALT and AST were also increased in *Trim56*-HepKO mice (Figure 3E-3F). To dissect the molecular mechanism of *Trim56* in NAFLD, we performed RNA-sequencing analysis in WT and *Trim56*-HepKO mouse liver. Our data revealed that pathways of fatty acid biosynthesis, lipid metabolism, and steroid metabolism are overrepresented in *Trim56*-HepKO mouse liver tissues (Figure 3G-3J).

Given the impact of *Trim56* deletion on augmented lipid metabolism-associated signaling pathways in hepatocytes, we next investigated the effect of hepatocyte-specific *Trim56*-overexpression on NAFLD pathogenesis. We generated *Trim56* hepatocyte-specific overexpressing mice (*Trim56*-HepOE) using the Sleeping Beauty Transpose system (16) and subjected them to HFD challenge. We observed that TRIM56 is successfully overexpressed and *Trim56*-HepOE mice displayed protection against NAFLD evidenced by decreased liver weight, and hepatic lipid accumulation (Figure 3K-3N). Serum levels of TC, ALT and AST were also lowered in *Trim56*-HepOE mice (Figure 3O-3P).

Identification of FASN as a TRIM56 binding partner

To gain insight into the possible mechanism of TRIM56 in regulating NAFLD, we first performed an integrative analysis of reported TRIM56 interactomics (BioGrid) and transcriptomic profiling in *Trim56*-HepKO liver tissues, which yielded FASN as the top hit based on integrated score ranking (Figure 4A-4C). Integrative analysis of reported TRIM56 interactomics and transcriptomic profiling in *Trim56*-KO mouse hepatocytes yielded similar results (Figure 4D-4E). By western blot analysis, we demonstrated FASN protein expression was decreased in primary mouse hepatocytes as well as human hepatocyte cell lines overexpressing TRIM56 (Figure 4F-4G). In contrast, increased expression of FASN as well as proteins in downstream lipogenesis cascades in the pathogenic process of fatty acid metabolism was observed in both liver tissues from *Trim56*-HepKO mice as well as in primary hepatocytes obtained from *Trim56*-KO mice (Figure 4H-4I), compared to respective controls.

TRIM56 interacts with FASN and promotes its degradation

Based on the above observations, it is plausible that TRIM56 interacts with FASN and promotes its degradation. We thus characterized the interaction between TRIM56 and FASN. By coimmunoprecipitation and GST pulldown assays, we found that TRIM56 interacted with FASN (Figure 5A-5E). Surface plasmon resonance (SPR) analysis further supported that TRIM56 directly interacted with FASN (Figure 5F). Structurally, TRIM56 consists of a highly conserved RING domain, two B-boxes, and a coiled-coil (CC) domain, and the C-terminal domain (CTD) that confers function specificity. We then mapped the interaction domain of TRIM56 using different versions of truncated TRIM56 fragments and confirmed that amino acids 522-755 of TRIM56 were essential for the interaction between TRIM56 and FASN, as demonstrated by the loss of the interaction between TRIM56 (1-521aa) and FASN (Figure 5G). Of functional

relevance, overexpression of full length TRIM56, but not TRIM56 (1-521aa), the non-FASN interacting TRIM56 fragment, reduces intracellular TG accumulation as lipid accumulation in hepatocytes (Figure 5H-5I). Further, we show that TRIM56 (1-521aa) overexpression did not lead to the downregulation of FASN or its downstream proteins associated with fatty acid metabolism. Furthermore, TRIM56 (1-521aa) overexpression also has no impact on the expression of lipogenesis-related gene expression (Figure 5J-5K).

To further address the molecular mechanisms underlying TRIM56-mediated FASN degradation, we overexpressed FLAG-TRIM56 and treated hepatocytes with chloroquine (CQ, a pharmacological inhibitor of lysosome-dependent protein degradation) or MG123 (an inhibitor of proteasome-dependent protein degradation). The western blot analysis results showed that TRIM56 overexpression-induced FASN downregulation was rescued by MG132 rather than CQ, suggesting that proteasome-dependent degradation of FASN may play a major role (Figure 6A). Compared with cells treated with empty vector, overexpression of TRIM56 led to enhanced FASN polyubiquitination (Figure 6B-6C). Given that multiple sites existing in ubiquitin give rise to substrate ubiquitination, we examined the specific site of ubiquitination involved. We identified that K48-linked polyubiquitination played a major role in the polyubiquitination of FASN (Figure 6D), which was further corroborated by the evidence showing increased FASN ubiquitination in K48O-overexpressing but not K48R-overexpressing cells (Figure 6E). However, deletion of the CTD of TRIM56 abrogated the TRIM56-FASN interaction, suggesting that CTD (522-755aa) of TRIM56 interacts with FASN. Overexpression of the TRIM56 (1-521aa) fragment (which is unable to bind with FASN) failed to increase FASN polyubiquitination, suggesting that amino acid position 522-575 is critical for TRIM56-FASN interaction and FASN protein instability (Figure 6F). More importantly, we demonstrated that, compared with the wild-type TRIM56, TRIM56

(21AACC24) (an E3 ubiquitin ligase activity defective mutant) (15) fails to increase FASN protein ubiquitination (Figure 6G). Consistent with this observation, wild-type TRIM56, but not TRIM56 (21AACC24) mutant decreases PO-induced lipid accumulation and TG elevation (Figure 6H-6I). TRIM56 (21AACC24) does not affect lipogenesis-related gene and protein expression (Figure 6J-6K). Altogether, these lines of evidence demonstrate that TRIM56 keep hepatocyte steatosis in check by interacting with FASN and conjugates K48-linked ubiquitination chains to promotes the degradation of FASN.

FASN inhibition blocks the effect of *Trim56* ablation on lipid accumulation

Given that FASN is required for *de novo* lipogenesis pathway, it remains to be elucidated whether FASN upregulation contributes to the altered lipid metabolism in *Trim56*-KO hepatocytes. We therefore asked whether decreasing FASN expression by shRNA-mediated knockdown or pharmacological inhibition of FASN activity by treatment with compound C75 could rescue the phenotype of *Trim56*-deficient hepatocytes upon metabolic challenge. We observed that sh*Fasn* significantly reduced FASN protein abundance (Figure 7A) and diminished TG accumulation in *Trim56*-KO hepatocytes (Figure 7B). FASN depletion also reversed the effect of *Trim56* deficiency on lipid droplet accumulation (Figure 7C) as well as the expression of genes involved in lipogenesis, fatty acid transport and elongation (such as *Scd1*, *Elovl5* and *Elovl6*) (Figure 7D). Likewise, pharmacological inhibition of FASN by compound C75 (17) also decreased FASN protein expression and reversed the effect of *Trim56* deficiency on lipid droplet formation and TG accumulation (Figure 7E-7G). We further performed RNA-sequencing analysis of primary hepatocytes isolated from wild-type and *Trim56*-KO mice treated with or without C75. Our data vividly demonstrated upregulation of enriched pathways in fatty acid

biosynthesis, lipid metabolism and steroid metabolism. However, treatment with C75 nullified the deleterious effects of *Trim56* deficiency by reversing the activation of these pathways as well as the deregulated gene expression (Figure 7H-7J). These results indicate that direct interaction between TRIM56 and FASN is required for hepatic lipid accumulation and that the TRIM56/FASN axis may serve to integrate critical mechanistic nodes linking metabolic stress and NAFLD development.

Artificial intelligence (AI)-based compound screening identifies FASstatin as an inhibitor of FASN

Searching for pharmacotherapies targeting NAFLD is an unmet medical need. Therapeutic targeting of protein degradation is an important strategy for NAFLD based on the nature of NAFLD as a spectrum of diseases characterized by nutrient surplus (18, 19). FASN is recognized as a master regulator of NAFLD pathogenesis, thus degradation of FASN protein expression or inhibition of FASN enzyme activity can lead to the suppression of hallmark events in NASH (*e.g.*, fatty acid metabolism, fibrogenesis and lobular inflammation) (20, 21). To identify lead compounds that promote FASN degradation as a protype of FASN inhibitors (FASNi), we performed an AI-based screening of a drug library consisting of 1.2 billion small-molecule compounds (Figure 8A). After the screening, we selected 14 compounds for further validation using PO-challenged human hepatocytes (Figure 8B). FASNi#8 (renamed FASstatin, chemical structure in 8C) stands out in this screening assay, as evidenced by diminished lipid droplet formation in human hepatocytes cell line. Molecular docking analysis suggested that FASstatin might have a binding mode with FASN protein (Figure 8D). Surface plasmon resonance (SPR) analysis reveals that FASstatin directly binds FASN ($Kd=1.6\times10^{-5}M$) (Figure 8E). As an

alternative approach to validate the direct interaction between FASstatin and FASN, we generated FASstatin linked with a biotin tag (Bio-FASstatin). Pulldown assay indicates that FASstatin binds FASN (Figure 8F). However, only wild type FASN can bind FASstatin, as mutation of two predicted key residues of FASN (Glu 2251 and Tyr2343) yields negative binding mode with FASstatin (Figure S3). We then explored the pharmacological actions of FASstatin. Our data demonstrated that FASstatin was not toxic to human hepatocyte cell line at concentrations up to 40 μM (Figure 8G). We next compared the efficacy of FASstatin with the currently used FASN inhibitor C75, and observed that FASstatin has higher suppressive effects on FASN protein expression, comparable FASN enzyme inhibition, and higher efficacy in suppressing lipid droplet formation (Figure 8H-8K). Since TRIM56 is a E3 ligase that promotes FASN protein degradation, we evaluated the possibility of whether FASstatin promotes TRIM56 dependent FASN ubiquitination. Intriguingly, we observed that TRIM56/FASN interaction and TRIM56-mediated FASN K48-linked polyubiquitination was significantly increased by FASstatin treatment (Figure 8L-8N). Of functional relevance, FASstatin treatment reversed the PO-induced lipid accumulation trigged by *TRIM56* depletion (Figure 8O).

FASstatin protects against NAFLD with good safety and oral bioavailability

To evaluate the therapeutic efficacy of FASstatin against NAFLD in mice, we established NAFLD in mice fed a HFD for 16 weeks and then FASstatin was orally administered (50 mg/kg/d) in to mice while continuing the HFD for an additional 8 weeks. The dose of FASstatin was selected based on a pilot study with escalating doses of FASstatin (0, 25, 50, 100 mg/kg/d) (Figure S4). The liver weight and body weight were increased after HFD feeding. However, pharmaceutical intervention with FASstatin significantly decreased FASN protein expression in

mouse liver but not in white adipose tissue, and reverted HFD-induced increases in liver weight and body weight, but not the weight of while adipose tissue (Figure 9A-9C). Histologically, photomicrographs of H&E and Oil Red O-stained sections revealed micro- and macrovesicular fat deposition and hepatocellular ballooning were reduced in mice receiving FASstatin treatment (Figure 9D). Also, liver TG, serum TC, TG, ALT and AST levels were lowered by FASstatin treatment (Figure 9E-9G). Next, we performed a pharmacokinetic study in mice. Our data reveal that FASstatin was orally bioavailable and has a bioavailability of 40.4% when given orally at dosage of 50 mg/kg (Figure 9H). We then determined the safety profile of FASstatin and characterized its safety profile in mice. Our data suggest that FASstatin does not affect the level of UREA and CK-MB, established biomarkers associated with kidney and myocardial injury. No apparent histological difference was observed between vehicle and FASstatin-treated mice (repeated dosing of FASstatin at 50 mg/kg/d for 8 weeks) (Figure S5A-S5B). In the acute toxicity test, mice can tolerate FASstatin at 1.75 g/kg after single-dose administration. FASstatin (single-dose at 1.75 g/kg) does not affect body weight and the weight of liver, kidney, heart, lung and spleen. FASstatin also has no significant effects on the levels of AST, AST, CREA, CK and LDH, established biomarkers associated with liver, kidney and myocardial injury. No apparent histological difference or damage of tissue was observed between vehicle and FASstatin-treated mice (single-dose at 1.75 g/kg) (Figure S5C-S5E). To further investigate the molecular mechanisms underlying the histopathological improvements mediated by FASstatin, we performed transcriptomic profiling on vehicle- and FASstatin-treated liver tissues. Our results indicate that enriched pathways in lipid metabolism and fatty acid biosynthesis was attenuated by FASstatin treatment (Figure 9I-9K).

To further explore the therapeutic potential of FASstatin in advanced stage of NAFLD-NASH, we established NASH model by feeding mice with a choline-deficient HFD (CDAHFD), a well-established model which exhibits characteristics of human NASH including hepatic steatosis, liver damage and fibrosis (22, 23). Our data demonstrate that FASstatin significantly decreased FASN protein expression (Figure 9L), reduced body or liver weight (Figure 9M), as well as attenuated hepatic steatosis, fibrosis and inflammation as well as decreasing serum ALT and AST activity (Figure 9N-9O). Based on the weight of evidence presented above and its safety and efficacy profile, FASstatin may serve as an orally bioavailable and well tolerated lead compound to block NAFLD/NASH development.

Discussion

NAFLD is the most prevalent form and etiological factor of metabolic liver disease affecting 25.2% of the general population (24). The number of people affected is ever increasing due to its silent nature and insufficient attention. The associated health-care burden continues to rise worldwide including China (25, 26). However, there are still no effective pharmacotherapies approved by the US Food and Drug Administration to treat NAFLD despite the fact that weight loss and lifestyle modification are beneficial (20, 21). Although some drug candidates have shown promising therapeutic effects in preclinical studies and have entered the therapeutic pipeline, most of these drugs have failed to achieve histological endpoints of NAFLD/NASH (20, 21). Due to the high prevalence and silent nature of NAFLD as well as adverse clinical outcomes which necessitates liver transplantation, there is an unmet medical need to identify effective therapeutic targets and pharmacotherapies for NAFLD/NASH. Regulatory pathways of protein homeostasis represent a promising avenue to address the metabolic overload nature of

NAFLD. FASN is a multi-functional protein target in NAFLD due to its purported role in *de novo* lipogenesis, liver inflammation, and fibrogenesis. Targeted degradation of FASN by E3-ligase is an appealing therapeutic approach in NAFLD therapeutics. Here, we describe a TRIM56/FASN axis that regulates hepatocyte lipid accumulation and lipotoxicity. Our data suggest that TRIM56 downregulation may thus serve as a converging point by which overnutrition and steatosis contribute to liver damage. In addition, AI-assisted drug discovery yields the discovery of a small-molecule inhibitor of FASN, FASstatin, which boosts TRIM56-FASN interaction and increases TRIM56-deriven FASN degradation and thus ameliorates NAFLD/NASH pathologies in mice with good efficacy, safety and pharmacokinetic profiles. These results suggest the potential to therapeutically target TRIM56/FASN axis in NAFLD.

Via multilayer screening, we identified the conserved enrichment of TRIM family in mouse and human NAFLD. TRIM is a protein family belonging to E3 ubiquitin ligases. Members of TRIM family can be induced by virus infection and are recognized as important regulators of antiviral defense and host innate immunity (27). Hepatocytes are essential for innate immune response by sensing and responding to physiological, pathophysiological, and environmental cues (28). Emerging evidence has convincingly demonstrated that hepatocytes are immune sentinels that sense and respond to immune, inflammatory and metabolic insults. In the scenario of metabolic liver disease, it has been reported that loss-of-function mutations in the peroxisomal/nuclear protein TRIM37 cause a monogenic multiorgan disorder characterized by metabolic syndrome (29, 30). FASN is one of the most attractive targets for NAFLD given its role in controlling driving mechanisms of NASH, *i.e.*, hepatic *de novo* lipogenesis (DNL), inflammatory and fibrogenic pathways (31, 32). However, the regulatory mechanisms of FASN in NAFLD and potential therapeutic strategies targeting FASN remain largely

unknown. Sorting nexin (SNX8) was found to mediate FASN protein degradation by recruiting TRIM28 and enhancing the TRIM28-FASN interaction (33). In addition, Yan *et al*. reported that TRIM8 expression was increased in liver tissues from patients with NAFLD/NASH. Mechanistic investigations have revealed that TRIM8 promotes NAFLD/NASH development by directly interacting with and ubiquitinating transforming growth factor-beta-activated kinase 1 (TAK1), thus promoting TAK1 phosphorylation and the ensuing activation of the JNK/p38 and NF-κB signaling pathways (34). Likewise, a more recent study has shown that TRIM16 attenuates hepatocyte steatosis and inflammation in a mouse NASH model by directly interacting with phosphorylated form of TAK1 and promote its degradation, leading to suppressed NASH development (16). Two more recent studies have demonstrated that TRIM31 alleviates NAFLD and NASH pathologies by targeted degradation of rhomboid 5 homolog 2 (Rhbdf2) (35) and transforming growth factor-beta-activated kinase 1 (TAK1) (36) in the liver. TRIM31 is also responsible for the anti-fibrotic effects of mulberrin (a bioactive phytochemical from traditional Chinese medicine Romulus Mori) in CCl_4-induced liver fibrosis (37). These lines of evidence illustrate the therapeutic potential of targeting TRIM family members in different stages of NAFLD. By employing unsupervised siRNA library screening of TRIM family proteins involved in hepatic steatosis, we revealed that TRIM56, an established RING-type E3 ubiquitin ligase in innate antiviral immunity (15, 27), as the most notable suppressor of PO-induced lipid accumulation.

Using unbiased protein interactomics screening and molecular validation, TRIM56 was found to directly interact with FASN, a key lipogenesis factor driving hepatic steatosis in NAFLD/NASH. The increased lipid accumulation in *Trim56* knockout hepatocytes promoted by PO treatment can be prevented by genetic depletion or pharmacological inhibition of FASN, suggesting that FASN

is a key downstream factor that regulates *Trim56* deficiency in hepatocytes. Overall, the spectrum of research data gleaned for TRIM56 was directionally congruent with the hepatoprotective role of TRIM56 in counteracting the pathophysiology of NAFLD.

Currently, some FASN inhibitors, such as platensimycin (38) has been shown to intervene in NAFLD progression in mouse models. Fortunately, some FASN inhibitors, such as TVB-2640 (32), a first-in-class and orally bioavailable FASN inhibitor, has undergone phase II clinical trials with significant effects in reducing liver fat and improving biochemical, inflammatory, and fibrotic biomarkers after 12 weeks of treatment. FT-4101 (39), another FASN inhibitor, is also in clinical development. These promising evidences gleaned from preclinical and clinical studies prompt us to identify potential FASN inhibitors. To effect clinical translation, by using a structure-guided approach, we discovered a small-molecule inhibitor of FASN, FASstatin. It outperforms C75, the first-generation FASN-targeting drug, in promoting FASN degradation. The effect of FASstatin at tested concentration possibly derives from dual mechanism including inhibition of FASN enzyme activity as well as FASN protein degradation. Based on the pharmacology data of FASstatin, this drug candidate appears more likely as a proteolysis targeting drug to reduce FASN protein expression. Further in-depth studies are needed to validate the contribution of FASN enzyme inhibition vs protein degradation to the observed pharmacological actions of FASstatin in vivo. FASstatin boosts the interaction between TRIM56 and FASN, leading to FASN inhibition in hepatocytes. Furthermore, our in vivo data demonstrate that inhibition of FASN by FASstatin reduces both circulating and hepatic levels of TC and TG. Most importantly, FASstatin was orally bioavailable and well tolerated in mice. Oral administration of FASstatin in HFD-induced NAFLD in mice leads to improved NAFLD pathologies. These pharmacological features suggests that the

effects of FASstatin on NAFLD could be different from ACC inhibitors, which has been shown to lower hepatic TG levels but to increase circulating TG levels (40, 41).

In light of the multifaceted roles of FASN in fatty acid synthesis, lipid metabolism and infection, pharmacological inhibition of FASN could also offer other extended protective effects, such as anti-aging (42), inhibition of HCC (43) as well as SARS-CoV-2 replication (33) etc. Additional work will be necessary to verify whether FASstatin could also exhibit pleiotropic protective effects in these diseases. Also, beyond its canonical role in innate immunity (such as cGAS/STING pathway) (44, 45), TRIM56 may also execute pivotal metabolic regulatory effects in immunity-independent manner. In addition, only male mice were used in the current study. However, female mice, typically resistant to HFD-induced obesity and NAFLD, can develop full NAFLD characteristics under thermoneutral housing conditions (46), further studies are warranted to elucidate the effects of FASstatin on NAFLD in female mice. Lastly, the doses of FASstatin in cultured cells is much higher than drug concentration in mouse serum. This is because in vivo and in vitro systems are different, and serum drug concentrations cannot be directly equivalent to the drug concentrations in cultured cells; The duration and frequency of drug administration, drug metabolites, drug solubility and permeability, cell type involved and the liver microenvironment are all important factors affecting the efficacy of the drug. Detailed characterization of the FASstatin pharmacology and tissue distribution is warranted in future studies.

In summary, we demonstrate that hepatocyte derived TRIM56 played a central role in maintaining metabolic homeostasis in the context of NAFLD. Thus, our work provides the proof-of-concept that pharmaceutical intervention of the TRIM56/FASN axis could be a

clinically translatable approach to rescue the systemic deregulated lipid metabolism observed in NAFLD.

Methods

Animal study

Mice were randomized into each group by randomization table. All animal studies were performed in accordance with Institutional Animal Care and Use Committee of University of Science and Technology of China (Approval number: USTCACUC212401038) and Renmin Hospital of Wuhan University (Approval number: WDRM20201207A). Reporting of the animal studies is in compliance with Animal Research: Reporting of In Vivo Experiments (ARRIVE) guidelines 2.0 listed in the Enhancing the QUAlity and Transparency Of health Research (EQUATOR) Network library.

Collection of human tissue sample

Human fatty liver samples were obtained from individuals with NAFLD who underwent liver biopsy. Patients with NAFLD due to viral infection, autoimmune hepatitis, excessive alcohol use (140 g/week for men or 70 g/week for women) were excluded for analysis. The NAFLD-free control samples were obtained from normal donors undergoing liver surgery. All the individuals enrolled in this study were excluded of drug abuse, hepatitis virus infection or excessive alcohol consumption. Liver histology was evaluated by two independent liver pathologists blinded to patients' demographical and other clinical data. NAFLD activity score (NAS) was evaluated according to the NASH-Clinical Research Network Scoring System criteria (47, 48).

Statistics

Data are presented as the mean ± SEM if data are normally distributed. For data that are not normally distributed, data are presented as the median and interquartile range (IQR). Before statistical analysis, data normality was assessed by the Shapiro-Wilk test. For data that are normally distributed, unpaired two-tailed Student's t-test was used to calculate statistical differences between 2 groups. For comparisons among multiple groups, one-way ANOVA followed by the Bonferroni post hoc test was used for data with homogeneity of variance. For data that does not follow normal distribution, a non-parametric test (Mann-Whitney U test for two groups; Kruskal-Wallis test for multiple groups) was applied for statistical analysis. In the one-way ANOVA analysis, Tamhane's T2 analysis was used when heteroscedasticity was observed. Statistical analysis was performed using SPSS Statistics v. 21.0. A P value of less than 0.05 was considered to be statistically significant. All images shown without biological replicates are representative of a minimum of three independent experiments.

An expanded method section is available in online data supplement.

Study approval

Human sample collection and use comply with the Ethics Committee of Renmin Hospital of Wuhan University (Approval number: WDRY2019-K011) and the First Affiliated Hospital of University of Science and Technology of China (Approval number: 2023KY-383). The study protocol conforms to the ethical guidelines of the 1975 Declaration of Helsinki. Written informed consent was obtained from each participant for collection of samples.

Data availability

All RNA-sequencing data support the findings of this study have deposited in NCBI Sequence Read Archive (SRA) with accession number: PRJNA1011487, PRJNA1011905 and PRJNA1011918. All remaining data that support the findings of this study are available in the main text or the supplemental materials. File of supporting data values for main figures and supplemental figures is available in online data supplements.

Author Contributions:

Conceptualization: JW

Methodology: SX, XW, SW, MX

Investigation: SX, XW, SW, MX, MC, JF, JG, TT, XC, JZ, ZW, ZW, YY

Funding acquisition: JW, YXJ, SX

Project administration: SX, XW, SW, XM, HY, ST, XM, TF, ZW

Supervision: JW, SX, XJZ

Writing – original draft: SX

Writing – review & editing: WX, FX, JY, SL, XJZ

Acknowledgments: We thank the members of Weng laboratory for critical discussion and constructive feedback. We are grateful to Fengjiao Hu, Xu Cai, Heng Hu and Yan Zhou for expert technical assistance in histological, pharmacokinetic, bioinformatic, molecular biology and transgenic mouse generation. This study was supported by grants from the National Key R&D Program of China (2021YFC2500500), the National Natural Science Foundation of China (82070464, 82370444, 82070079 and 82370395), Anhui Provincial Key Research and

Development Program (202104j07020051) and Anhui Provincial Natural Science Foundation (2208085J08).

Competing interests: Authors declare that they have no competing interests.

References

1. Powell EE, Wong VW, and Rinella M. Non-alcoholic fatty liver disease. *Lancet (London, England).* 2021;397(10290):2212-24.
2. Eslam M, Newsome PN, Sarin SK, Anstee QM, Targher G, Romero-Gomez M, et al. A new definition for metabolic dysfunction-associated fatty liver disease: An international expert consensus statement. *Journal of hepatology.* 2020;73(1):202-9.
3. Rinella ME, Lazarus JV, Ratziu V, Francque SM, Sanyal AJ, Kanwal F, et al. A multi-society Delphi consensus statement on new fatty liver disease nomenclature. *Journal of hepatology.* 2023. doi: 10.1016/j.aohep.2023.101133.
4. Bugianesi E, and Petta S. NAFLD/NASH. *Journal of hepatology.* 2022;DOI: 10.1016/j.jhep.2022.02.006.
5. Cazanave SC, Warren AD, Pacula M, Touti F, Zagorska A, Gural N, et al. Peptide-based urinary monitoring of fibrotic nonalcoholic steatohepatitis by mass-barcoded activity-based sensors. *Science translational medicine.* 2021;13(616):eabe8939.
6. Lazarus JV, Mark HE, Anstee QM, Arab JP, Batterham RL, Castera L, et al. Advancing the global public health agenda for NAFLD: a consensus statement. *Nature reviews Gastroenterology & hepatology.* 2022;19(1):60-78.
7. Brunt EM, Wong VW, Nobili V, Day CP, Sookoian S, Maher JJ, et al. Nonalcoholic fatty liver disease. *Nature reviews Disease primers.* 2015;1:15080.
8. Piccinin E, Villani G, and Moschetta A. Metabolic aspects in NAFLD, NASH and hepatocellular carcinoma: the role of PGC1 coactivators. *Nature reviews Gastroenterology & hepatology.* 2019;16(3):160-74.
9. Cariou B, Byrne CD, Loomba R, and Sanyal AJ. Nonalcoholic fatty liver disease as a metabolic disease in humans: A literature review. *Diabetes, obesity & metabolism.* 2021;23(5):1069-83.
10. Perdomo CM, Frühbeck G, and Escalada J. Impact of Nutritional Changes on Nonalcoholic Fatty Liver Disease. *Nutrients.* 2019;11(3).
11. Hatakeyama S. TRIM Family Proteins: Roles in Autophagy, Immunity, and Carcinogenesis. *Trends in biochemical sciences.* 2017;42(4):297-311.
12. Watanabe M, and Hatakeyama S. TRIM proteins and diseases. *Journal of biochemistry.* 2017;161(2):135-44.
13. Wu L, Yin X, Jiang K, Yin J, Yu H, Yang L, et al. Comprehensive profiling of the TRIpartite motif family to identify pivot genes in hepatocellular carcinoma. *Cancer medicine.* 2022;11(7):1712-31.
14. Qian H, and Chen L. TRIM proteins in fibrosis. *Biomedicine & pharmacotherapy = Biomedecine & pharmacotherapie.* 2021;144:112340.

15. Wang J, Liu B, Wang N, Lee YM, Liu C, and Li K. TRIM56 is a virus- and interferon-inducible E3 ubiquitin ligase that restricts pestivirus infection. *Journal of virology.* 2011;85(8):3733-45.
16. Wang L, Zhang X, Lin ZB, Yang PJ, Xu H, Duan JL, et al. Tripartite motif 16 ameliorates nonalcoholic steatohepatitis by promoting the degradation of phospho-TAK1. *Cell metabolism.* 2021;33(7):1372-88.e7.
17. Thupari JN, Landree LE, Ronnett GV, and Kuhajda FP. C75 increases peripheral energy utilization and fatty acid oxidation in diet-induced obesity. *Proceedings of the National Academy of Sciences of the United States of America.* 2002;99(14):9498-502.
18. Xia SW, Wang ZM, Sun SM, Su Y, Li ZH, Shao JJ, et al. Endoplasmic reticulum stress and protein degradation in chronic liver disease. *Pharmacological research.* 2020;161:105218.
19. Wu X, Xu M, Geng M, Chen S, Little PJ, Xu S, et al. Targeting protein modifications in metabolic diseases: molecular mechanisms and targeted therapies. *Signal transduction and targeted therapy.* 2023;8(1):220.
20. Yang YY, Xie L, Zhang NP, Zhou D, Liu TT, and Wu J. Updates on novel pharmacotherapeutics for the treatment of nonalcoholic steatohepatitis. *Acta pharmacologica* Sinica. 2022: 43(5):1180-1190
21. Batchuluun B, Pinkosky SL, and Steinberg GR. Lipogenesis inhibitors: therapeutic opportunities and challenges. *Nature reviews Drug discovery.* 2022:1-23.
22. Li Y, Xu J, Lu Y, Bian H, Yang L, Wu H, et al. DRAK2 aggravates nonalcoholic fatty liver disease progression through SRSF6-associated RNA alternative splicing. *Cell metabolism.* 2021;33(10):2004-20.e9.
23. Zhao P, Sun X, Chaggan C, Liao Z, In Wong K, He F, et al. An AMPK-caspase-6 axis controls liver damage in nonalcoholic steatohepatitis. *Science (New York, NY).* 2020;367(6478):652-60.
24. Younossi ZM, Koenig AB, Abdelatif D, Fazel Y, Henry L, and Wymer M. Global epidemiology of nonalcoholic fatty liver disease-Meta-analytic assessment of prevalence, incidence, and outcomes. *Hepatology (Baltimore, Md).* 2016;64(1):73-84.
25. Zhou J, Zhou F, Wang W, Zhang XJ, Ji YX, Zhang P, et al. Epidemiological Features of NAFLD From 1999 to 2018 in China. *Hepatology (Baltimore, Md).* 2020;71(5):1851-64.
26. Zhou F, Zhou J, Wang W, Zhang XJ, Ji YX, Zhang P, et al. Unexpected Rapid Increase in the Burden of NAFLD in China From 2008 to 2018: A Systematic Review and Meta-Analysis. *Hepatology (Baltimore, Md).* 2019;70(4):1119-33.
27. Shen Y, Li NL, Wang J, Liu B, Lester S, and Li K. TRIM56 is an essential component of the TLR3 antiviral signaling pathway. *The Journal of biological chemistry.* 2012;287(43):36404-13.
28. Zhou Z, Xu MJ, and Gao B. Hepatocytes: a key cell type for innate immunity. *Cellular & molecular immunology.* 2016;13(3):301-15.
29. Karlberg N, Jalanko H, Kallijärvi J, Lehesjoki AE, and Lipsanen-Nyman M. Insulin resistance syndrome in subjects with mutated RING finger protein TRIM37. *Diabetes.* 2005;54(12):3577-81.
30. Kettunen KM, Karikoski R, Hämäläinen RH, Toivonen TT, Antonenkov VD, Kulesskaya N, et al. Trim37-deficient mice recapitulate several features of the multi-organ disorder Mulibrey nanism. *Biology open.* 2016;5(5):584-95.
31. Menendez JA, and Lupu R. Fatty acid synthase and the lipogenic phenotype in cancer pathogenesis. *Nature reviews Cancer.* 2007;7(10):763-77.

32. Loomba R, Mohseni R, Lucas KJ, Gutierrez JA, Perry RG, Trotter JF, et al. TVB-2640 (FASN Inhibitor) for the Treatment of Nonalcoholic Steatohepatitis: FASCINATE-1, a Randomized, Placebo-Controlled Phase 2a Trial. *Gastroenterology.* 2021;161(5):1475-86.
33. Chu J, Xing C, Du Y, Duan T, Liu S, Zhang P, et al. Pharmacological inhibition of fatty acid synthesis blocks SARS-CoV-2 replication. *Nature metabolism.* 2021;3(11):1466-75.
34. Yan FJ, Zhang XJ, Wang WX, Ji YX, Wang PX, Yang Y, et al. The E3 ligase tripartite motif 8 targets TAK1 to promote insulin resistance and steatohepatitis. *Hepatology (Baltimore, Md).* 2017;65(5):1492-511.
35. Xu M, Tan J, Dong W, Zou B, Teng X, Zhu L, et al. The E3 ubiquitin-protein ligase Trim31 alleviates non-alcoholic fatty liver disease by targeting Rhbdf2 in mouse hepatocytes. *Nature communications.* 2022;13(1):1052.
36. Xu MX, Tan J, Ge CX, Dong W, Zhang LT, Zhu LC, et al. TRIM31 confers protection against nonalcoholic steatohepatitis by deactivating MAP3K7. *Hepatology (Baltimore, Md).* 2022.
37. Ge C, Tan J, Lou D, Zhu L, Zhong Z, Dai X, et al. Mulberrin confers protection against hepatic fibrosis by Trim31/Nrf2 signaling. *Redox biology.* 2022;51:102274.
38. Su M, Cao D, Wang Z, Duan Y, and Huang Y. Fatty Acid Synthase Inhibitor Platensimycin Intervenes the Development of Nonalcoholic Fatty Liver Disease in a Mouse Model. *Biomedicines.* 2021;10(1).
39. Beysen C, Schroeder P, Wu E, Brevard J, Ribadeneira M, Lu W, et al. Inhibition of fatty acid synthase with FT-4101 safely reduces hepatic de novo lipogenesis and steatosis in obese subjects with non-alcoholic fatty liver disease: Results from two early-phase randomized trials. *Diabetes, obesity & metabolism.* 2021;23(3):700-10.
40. Calle RA, Amin NB, Carvajal-Gonzalez S, Ross TT, Bergman A, Aggarwal S, et al. ACC inhibitor alone or co-administered with a DGAT2 inhibitor in patients with non-alcoholic fatty liver disease: two parallel, placebo-controlled, randomized phase 2a trials. *Nature medicine.* 2021;27(10):1836-48.
41. Zhang XJ, Cai J, and Li H. Targeting ACC for NASH resolution. *Trends in molecular medicine.* 2022;28(1):5-7.
42. Fafián-Labora J, Carpintero-Fernández P, Jordan SJD, Shikh-Bahaei T, Abdullah SM, Mahenthiran M, et al. FASN activity is important for the initial stages of the induction of senescence. *Cell death & disease.* 2019;10(4):318.
43. Du D, Liu C, Qin M, Zhang X, Xi T, Yuan S, et al. Metabolic dysregulation and emerging therapeutical targets for hepatocellular carcinoma. *Acta pharmaceutica Sinica B.* 2022;12(2):558-80.
44. Seo GJ, Kim C, Shin WJ, Sklan EH, Eoh H, and Jung JU. TRIM56-mediated monoubiquitination of cGAS for cytosolic DNA sensing. *Nature communications.* 2018;9(1):613.
45. Tsuchida T, Zou J, Saitoh T, Kumar H, Abe T, Matsuura Y, et al. The ubiquitin ligase TRIM56 regulates innate immune responses to intracellular double-stranded DNA. *Immunity.* 2010;33(5):765-76.
46. Giles DA, Moreno-Fernandez ME, Stankiewicz TE, Graspeuntner S, Cappelletti M, Wu D, et al. Thermoneutral housing exacerbates nonalcoholic fatty liver disease in mice and allows for sex-independent disease modeling. *Nature medicine.* 2017;23(7):829-38.
47. Kleiner DE, Brunt EM, Van Natta M, Behling C, Contos MJ, Cummings OW, et al. Design and validation of a histological scoring system for nonalcoholic fatty liver disease.

Hepatology (Baltimore, Md). 2005;41(6):1313-21.
48. Brunt EM, Kleiner DE, Wilson LA, Belt P, and Neuschwander-Tetri BA. Nonalcoholic fatty liver disease (NAFLD) activity score and the histopathologic diagnosis in NAFLD: distinct clinicopathologic meanings. *Hepatology (Baltimore, Md).* 2011;53(3):810-20.

Figures and Figure Legends

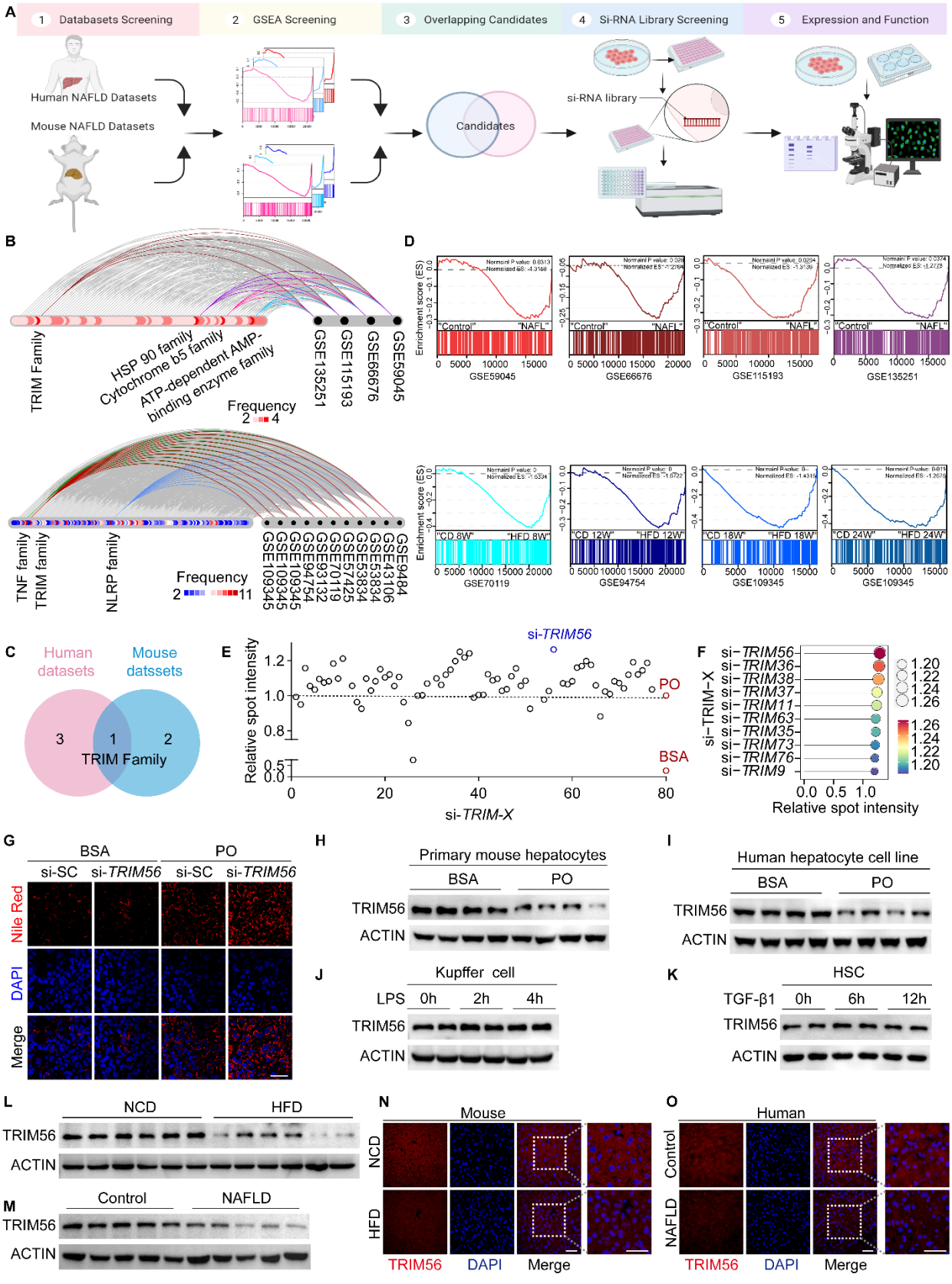
A
1 Databasets Screening
2 GSEA Screening
3 Overlapping Candidates
4 Si-RNA Library Screening
5 Expression and Function
Human NAFLD Datasets
Mouse NAFLD Datasets
Candidates
si-RNA library
B
TRIM Family
HSP 90 family
Cytochrome b5 family
ATP-dependent AMP-binding enzyme family
GSE135251
GSE115193
GSE66676
GSE59045
Frequency
2 4
TNF family
TRIM family
NLRP family
Frequency
2 11
D
Enrichment score (ES)
"Control"
"NAFL"
GSE59045
GSE66676
GSE115193
GSE135251
"CD 8W"
"HFD 8W"
"CD 12W"
"HFD 12W"
"CD 18W"
"HFD 18W"
"CD 24W"
"HFD 24W"
GSE70119
GSE94754
GSE109345
GSE109345
C
Human datasets
Mouse datsets
3
1
2
TRIM Family
E
si-TRIM56
PO
BSA
Relative spot intensity
si-TRIM-X
F
si-TRIM-X
si-TRIM56
si-TRIM36
si-TRIM38
si-TRIM37
si-TRIM11
si-TRIM63
si-TRIM35
si-TRIM73
si-TRIM76
si-TRIM9
Relative spot intensity
G
BSA
PO
si-SC
si-TRIM56
si-SC
si-TRIM56
Nile Red
DAPI
Merge
H
Primary mouse hepatocytes
BSA
PO
TRIM56
ACTIN
I
Human hepatocyte cell line
BSA
PO
TRIM56
ACTIN
J
Kupffer cell
LPS
0h
2h
4h
TRIM56
ACTIN
K
HSC
TGF-β1
0h
6h
12h
TRIM56
ACTIN
L
NCD
HFD
TRIM56
ACTIN
M
Control
NAFLD
TRIM56
ACTIN
N
Mouse
NCD
HFD
TRIM56
DAPI
Merge
O
Human
Control
NAFLD
TRIM56
DAPI
Merge

633

Fig. 1. Identification of TRIM56 as the key regulator of NAFLD

(A) Workflow for the discovery of key regulator(s) of NAFLD.

(B) Hive plot showing the top protein families associated with NAFLD in RNA-seq datasets from human (upper panel) and mouse (lower panel) NAFLD liver samples versus respective controls.

(C) Venn diagram showing conserved alterations of TRIM family members in individuals with NAFL and mouse models of NAFLD based on GEO datasets as described.

(D) Enrichment of TRIM family members in individuals with NAFL (upper panel) and in mouse with NAFLD after feeding with high fat diet for different weeks (lower panel) by GSEA.

(E) Scatterplot of Nile Red-stained lipid droplets content in palmitic acid (PA; 0.5 mM) and oleic acid (OA; 1.0 mM) (PO)-challenged human hepatocytes after knockdown the TRIM family members, n=4. Relative spot intensity to that of PO-challenged cells is presented.

(F) Lollipop chart of top 10 hit using average fold change as the readout.

(G) Representative images of Nile Red staining of TRIM56 knockdown by si-TRIM56 and the scramble control (si-SC) in HepG2 cell after PO or BSA stimulation, scale bar, 50 μm, n=3.

(H) Western blotting of TRIM56 in mouse primary hepatocytes that were treated with control (BSA) or PO for 18 h, n=4.

(I) Western blotting of TRIM56 in HepG2 treated with BSA or PO for 18 h, n=3. Four technical replicates were run for each independent experiment.

(J) Western blotting of TRIM56 in Kupffer cells that were treated with LPS (1 μg/ml) for indicated time periods, n=3. Technical replicates were run for each independent experiment.

(K) Western blotting of TRIM56 in isolated primary mouse hepatic stellate cells (HSCs) were treated with recombinant mouse TGF-β1 (10 ng/ml) for indicated time periods, n=3.

(L) Western blotting of TRIM56 in in liver tissues from mice fed with normal chow diet (NCD) or HFD for 24 weeks as determined by western blot analysis, n=6.

(M) Western blotting of TRIM56 in liver samples from individuals with NAFLD or control group, n=5.

(N) Representative immunofluorescence staining of TRIM56 in livers of HFD- and NCD-fed mice, n=6. Red, TRIM56. Blue, DAPI. Scale bar, 50 μm.

(O) Representative immunofluorescence staining of TRIM56 in liver tissues from individuals with NAFLD and normal control subjects, n=6. Red, TRIM56. Blue, DAPI. Scale bar, 50 μm.

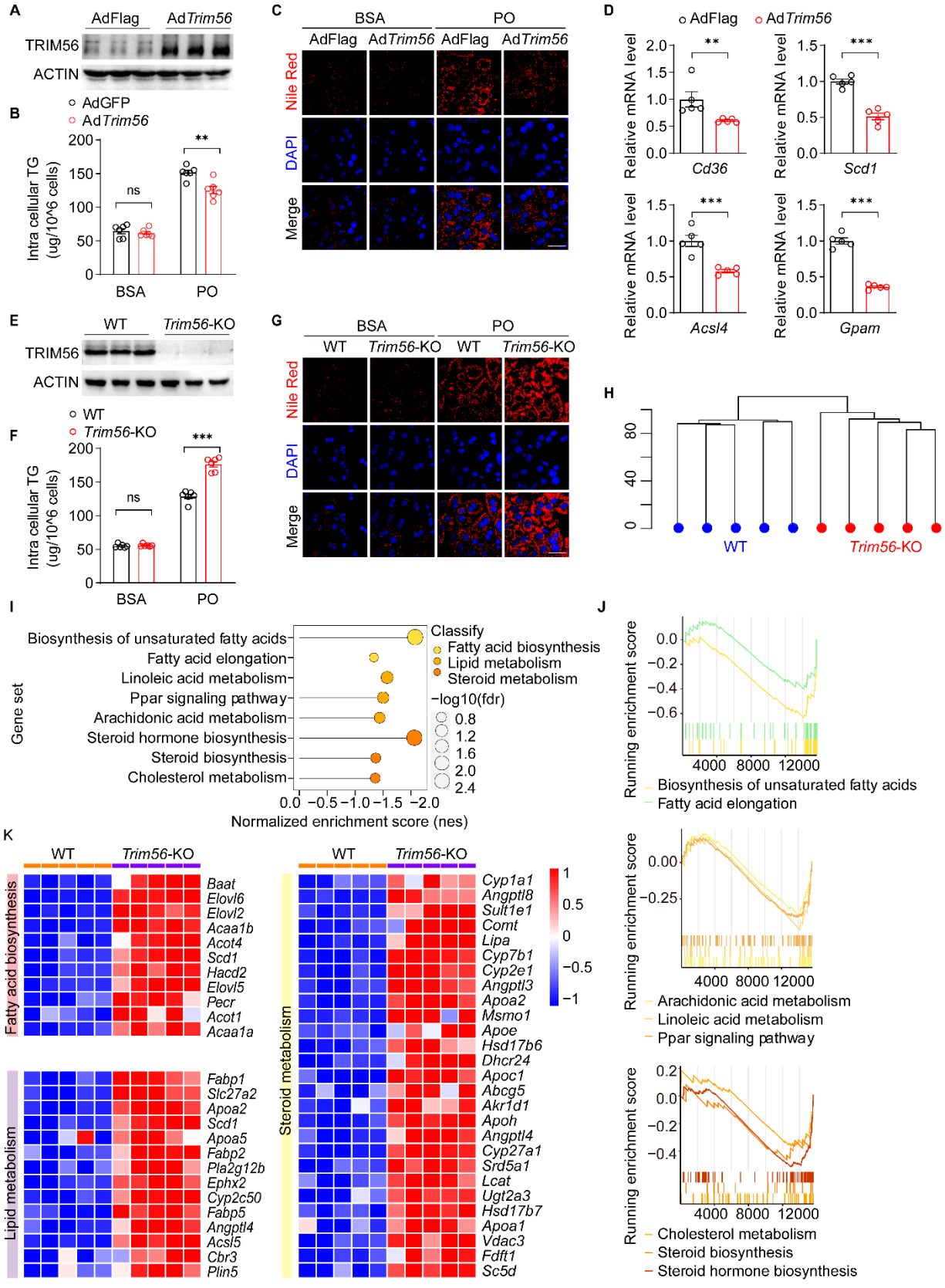
A
AdFlag
AdTrim56
TRIM56
ACTIN
B
AdGFP
AdTrim56
Intra cellular TG (ug/10^6 cells)
ns
**
BSA
PO
C
BSA
PO
AdFlag
AdTrim56
Nile Red
DAPI
Merge
D
AdFlag
AdTrim56
Relative mRNA level
Cd36
Scd1
Acsl4
Gpam
E
WT
Trim56-KO
TRIM56
ACTIN
F
***
G
H
WT
Trim56-KO
I
Biosynthesis of unsaturated fatty acids
Fatty acid elongation
Linoleic acid metabolism
Ppar signaling pathway
Arachidonic acid metabolism
Steroid hormone biosynthesis
Steroid biosynthesis
Cholesterol metabolism
Gene set
Classify
Fatty acid biosynthesis
Lipid metabolism
Steroid metabolism
−log10(fdr)
Normalized enrichment score (nes)
J
Running enrichment score
K
Fatty acid biosynthesis
Lipid metabolism
Steroid metabolism
Baat
Elovl6
Elovl2
Acaa1b
Acot4
Scd1
Hacd2
Elovl5
Pecr
Acot1
Acaa1a
Fabp1
Slc27a2
Apoa2
Scd1
Apoa5
Fabp2
Pla2g12b
Ephx2
Cyp2c50
Fabp5
Angptl4
Acsl5
Cbr3
Plin5
Cyp1a1
Angptl8
Sult1e1
Comt
Lipa
Cyp7b1
Cyp2e1
Angptl3
Apoa2
Msmo1
Apoe
Hsd17b6
Dhcr24
Apoc1
Abcg5
Akr1d1
Apoh
Angptl4
Cyp27a1
Srd5a1
Lcat
Ugt2a3
Hsd17b7
Apoa1
Vdac3
Fdft1
Sc5d

Fig. 2. TRIM56 blocks hepatocyte lipid accumulation

(A) Primary mouse hepatocytes were infected with control adenovirus (AdFlag) or *Trim56* adenovirus (Ad*Trim56*) for 24 h before western blot was performed to determine the extent of TRIM56 overexpression, n=3.

(B) Intracellular triglyceride (TG) level was determined in primary mouse hepatocytes infected with AdFlag or Ad*Trim56* in the presence of PO, n=6. One-way ANOVA followed by the Bonferroni post hoc test

(C) Primary mouse hepatocytes were infected with AdFlag or Ad*Trim56* in the presence of PO. Nile Red staining was performed to visualize lipid droplet accumulation, n=3. Scale bar, 50 μm.

(D) The relative mRNA levels of genes related to fatty acid metabolism (*Cd36*, *Scd1*, *Acsl4*, *Gpam*) in the indicated groups in the presence of PO, n=5. Mann-Whitney U test for *Cd36,* two-tailed Student's t-test for *Scd1*, *Acsl4*, *Gpam*,

(E) Validation of TRIM56 protein expression in hepatocytes isolated from wild type (WT) and *Trim56* global knockout (*Trim56*-KO) mouse, n=3.

(F) Primary hepatocytes were isolated from WT and *Trim56*-KO mice. Intracellular TG level was determined in PO-challenged primary hepatocytes, n=6. One-way ANOVA followed by the Tamhane's T2 analysis.

(G) WT or *Trim56*-KO hepatocytes were treated with PO for 18 h before Nile Red staining was performed to visualize lipid droplet accumulation, scale bar, 50 μm, n=3.

(H) Cluster profile of WT and *Trim56*-KO hepatocytes treated with PO, n=5.

(I) Enriched pathways in *Trim56*-KO hepatocytes vs WT hepatocytes treated with PO.

(J) GSEA analysis of pathways displayed in (I).

(K) Heatmap analysis of differentially expressed genes of WT and *Trim56*-KO hepatocytes treated

689 with PO by RNA-sequencing. Differentially expressed genes in pathways of lipid metabolism,
690 fatty acid metabolism and steroid metabolism are highlighted.
691 *$P < 0.05$， **$P<0.01$, and ***$P < 0.001$.
692

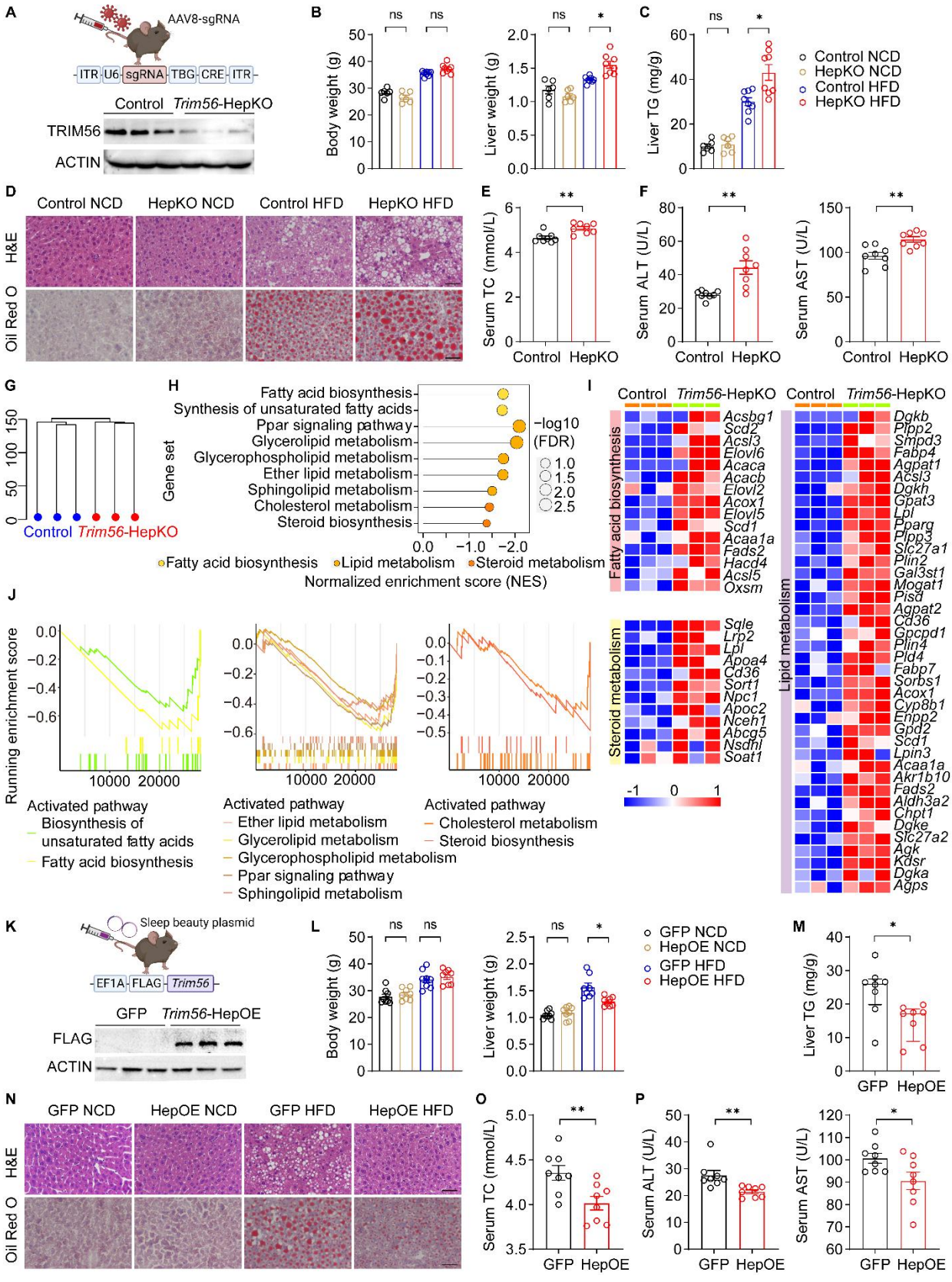
A
AAV8-sgRNA
ITR U6 sgRNA TBG CRE ITR
Control Trim56-HepKO
TRIM56
ACTIN
B
Body weight (g)
Liver weight (g)
ns
*
C
Liver TG (mg/g)
Control NCD
HepKO NCD
Control HFD
HepKO HFD
D
Control NCD
HepKO NCD
Control HFD
HepKO HFD
H&E
Oil Red O
E
Serum TC (mmol/L)
F
Serum ALT (U/L)
Serum AST (U/L)
**
Control HepKO
G
Control Trim56-HepKO
H
Fatty acid biosynthesis
Synthesis of unsaturated fatty acids
Ppar signaling pathway
Glycerolipid metabolism
Glycerophospholipid metabolism
Ether lipid metabolism
Sphingolipid metabolism
Cholesterol metabolism
Steroid biosynthesis
Gene set
−log10 (FDR)
Fatty acid biosynthesis
Lipid metabolism
Steroid metabolism
Normalized enrichment score (NES)
I
Control Trim56-HepKO
Fatty acid biosynthesis
Acsbg1 Scd2 Acsl3 Elovl6 Acaca Acacb Elovl2 Acox1 Elovl5 Scd1 Acaa1a Fads2 Hacd4 Acsl5 Oxsm
Steroid metabolism
Sqle Lrp2 Lpl Apoa4 Cd36 Sort1 Npc1 Apoc2 Nceh1 Abcg5 Nsdhl Soat1
Lipid metabolism
Dgkb Plpp2 Smpd3 Fabp4 Agpat1 Acsl3 Dgkh Gpat3 Lpl Pparg Plpp3 Slc27a1 Plin2 Gal3st1 Mogat1 Pisd Agpat2 Cd36 Gpcpd1 Plin4 Pld4 Fabp7 Sorbs1 Acox1 Cyp8b1 Enpp2 Gpd2 Scd1 Lpin3 Acaa1a Akr1b10 Fads2 Aldh3a2 Chpt1 Dgke Slc27a2 Agk Kdsr Dgka Agps
J
Running enrichment score
Activated pathway
Biosynthesis of unsaturated fatty acids
Fatty acid biosynthesis
Ether lipid metabolism
Glycerolipid metabolism
Glycerophospholipid metabolism
Ppar signaling pathway
Sphingolipid metabolism
Cholesterol metabolism
Steroid biosynthesis
K
Sleep beauty plasmid
EF1A FLAG Trim56
GFP Trim56-HepOE
FLAG
ACTIN
L
GFP NCD
HepOE NCD
GFP HFD
HepOE HFD
M
GFP HepOE
N
GFP NCD
HepOE NCD
GFP HFD
HepOE HFD
H&E
Oil Red O
O
P

Fig. 3. Hepatocyte TRIM56 protects against HFD-induced hepatic steatosis

(A) Scheme of generating hepatocyte-specific *Trim56* knockout mice (*Trim56*-HepKO) using AAV8-*Trim56*-sgRNA-TBG-Cre injection. Mice receiving AAV8-control sgRNA injection was used as the control. Successful deletion of TRIM56 protein in liver was verified by western blot analysis, n=3.

(B) Body weight and liver weight of WT and *Trim56*-HepKO after 16 weeks of HFD feeding, n=6 for normal chow diet (NCD), n=8 for HFD. One-way ANOVA followed by the Bonferroni post hoc test for body weight, Tamhane's T2 analysis for liver weight.

(C) Liver TG content in WT and *Trim56*-HepKO after 16 weeks of HFD feeding, n=6 for NCD, n=8 for HFD.

(D) Representative H&E and Oil Red O staining of the liver sections of the mice in the indicated group, scale bars, 50 μm, n=4.

(E) Serum TC content of WT and *Trim56*-HepKO after 16 weeks of HFD feeding, n=8, two-tailed Student's t-test

(F) Serum ALT and AST levels of the mice after 16 weeks of HFD feeding, n=8, two-tailed Student's t-test

(G) Cluster profile of WT and *Trim56*-HepKO mice fed with HFD for 16 weeks.

(H) Enriched pathway analysis of liver tissues from *Trim56*-HepKO mice vs control mice, n=3.

(I) Heatmap illustrating overrepresented pathways of fatty acid biosynthesis, lipid metabolism and steroid metabolism in liver tissues from *Trim56*-HepKO mice, n=3.

(J) GSEA analysis showing pathways of fatty acid biosynthesis, lipid metabolism and steroid metabolism are overrepresented in liver tissues from *Trim56*-HepKO mice, n=3.

(K) Scheme of generating hepatocyte-specific *Trim56* overexpressing mice (*Trim56*-HepOE) by

using *Trim56*-sleeping beauty plasmid injection. Control mice receive injection of empty vector. Successful deletion of TRIM56 protein in liver was verified by western blot analysis, n=3.

(L) Body weight and liver weight of WT (GFP) and *Trim56*-HepOE mice after 16 weeks of NCD or HFD feeding, n=8. One-way ANOVA followed by the Bonferroni post hoc test for body weight, Tamhane's T2 analysis for liver weight.

(M) Liver TG content in WT and *Trim56*-HepOE mice after16 weeks of HFD feeding, n=8. Mann-Whitney U test.

(N) Representative H&E and Oil Red O staining of the liver sections of the mice in the indicated group, scale bar, 50 μm, n=3.

(O) Serum TC content of WT and *Trim56*-HepOE mice after 16 weeks of HFD feeding, n=8, two-tailed Student's t-test

(P) Serum ALT and AST contents of WT and *Trim56*-HepOE mice after16 weeks of HFD feeding, n=8, two-tailed Student's t-test

$*P < 0.05$，$**P<0.01$, and $***P < 0.001$.

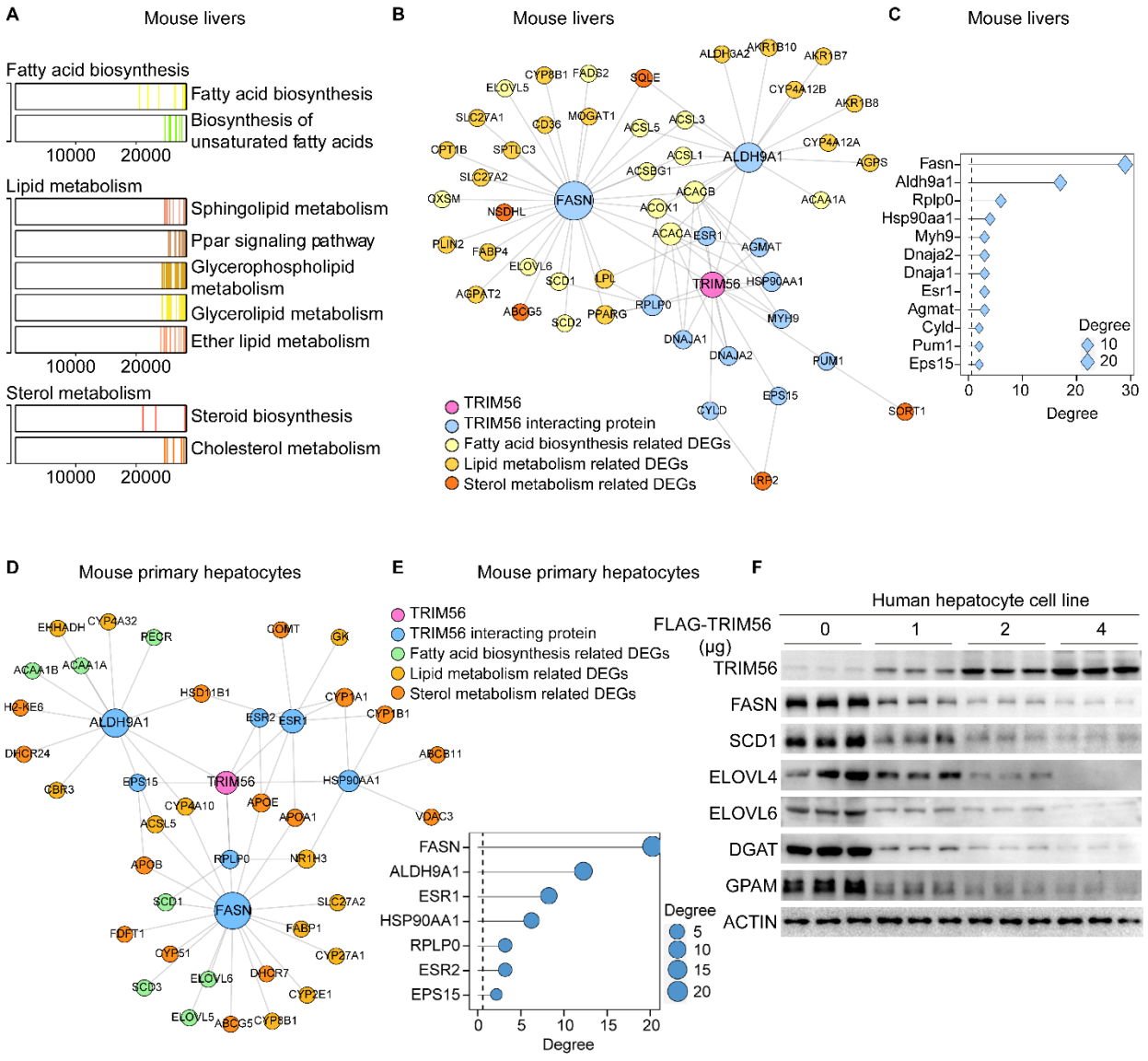
A
Mouse livers
Fatty acid biosynthesis
Fatty acid biosynthesis
Biosynthesis of unsaturated fatty acids
10000
20000
Lipid metabolism
Sphingolipid metabolism
Ppar signaling pathway
Glycerophospholipid metabolism
Glycerolipid metabolism
Ether lipid metabolism
10000
20000
Sterol metabolism
Steroid biosynthesis
Cholesterol metabolism
10000
20000
B
Mouse livers
TRIM56
TRIM56 interacting protein
Fatty acid biosynthesis related DEGs
Lipid metabolism related DEGs
Sterol metabolism related DEGs
C
Mouse livers
Fasn
Aldh9a1
Rplp0
Hsp90aa1
Myh9
Dnaja2
Dnaja1
Esr1
Agmat
Cyld
Pum1
Eps15
Degree
10
20
0
10
20
30
Degree
D
Mouse primary hepatocytes
E
Mouse primary hepatocytes
TRIM56
TRIM56 interacting protein
Fatty acid biosynthesis related DEGs
Lipid metabolism related DEGs
Sterol metabolism related DEGs
FASN
ALDH9A1
ESR1
HSP90AA1
RPLP0
ESR2
EPS15
Degree
5
10
15
20
0
5
10
15
20
Degree
F
Human hepatocyte cell line
FLAG-TRIM56 (μg)
0
1
2
4
TRIM56
FASN
SCD1
ELOVL4
ELOVL6
DGAT
GPAM
ACTIN
G
Mouse primary hepatocytes
Ad-Flag
Ad-Trim56
TRIM56
FASN
SCD1
ELOVL4
ELOVL6
DGAT
GPAM
ACTIN
H
Mouse livers
Control
Trim56-HepKO
TRIM56
ACTIN
FASN
SCD1
ELOVL4
ELOVL6
DGAT
GPAM
ACTIN
I
Mouse primary hepatocytes
WT
Trim56-KO
TRIM56
FASN
SCD1
ELOVL4
ELOVL6
DGAT
GPAM
ACTIN

732

Fig. 4. Identification of FASN as a TRIM56 binding partner

(A) Enriched pathway analysis in *Trim56*-HepKO mouse liver tissues revealed by RNA-sequencing.

(B) Integrated analysis of TRIM56 interactomics and RNA-seq of samples described in A.

(C) Ranking of candidate proteins interacting with TRIM56 in mouse liver tissues.

(D) Integrated analysis of TRIM56 interactomics and RNA-seq of samples from *Trim56*-KO hepatocytes.

(E) Ranking of candidate proteins interacting with TRIM56 in mouse hepatocytes.

(F) HepG2 were transfected with empty vector (FLAG) or increasing amount of FLAG-TRIM56 (0, 1, 2 and 4 μg) in the presence of PO before whole cell lysate was collected for western blot to determine proteins in lipogenesis pathway (SCD1, ELOVL4, ELOVL6, DGAT and GPAM), n=3.

(G) Primary mouse hepatocytes were infected with AdFlag or AdFlag-*Trim56* in the presence of PO before whole cell lysate was collected for western blot to determine the expression of proteins in lipogenesis pathway, n=4.

(H) Expression of FASN and downstream proteins associated with in lipogenesis pathway in WT and *Trim56*-HepKO mouse liver tissues under HFD conditions, n=6.

(I) Expression of FASN and downstream lipogenesis-related proteins in WT and *Trim56*-KO mouse hepatocytes treated with PO, n=4.

$*P < 0.05$， $**P<0.01$, and $***P < 0.001$.

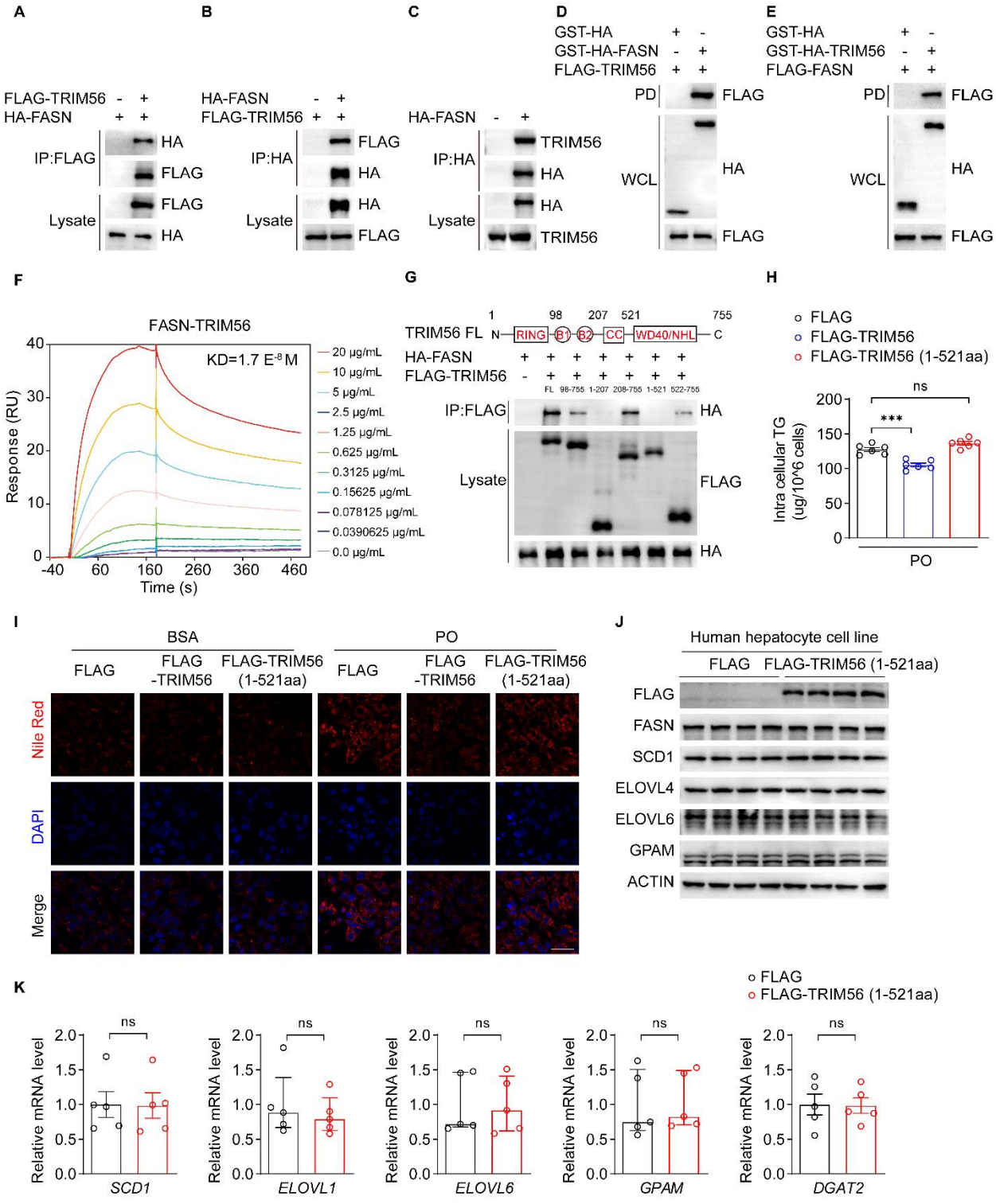
A
FLAG-TRIM56 - +
HA-FASN + +
IP:FLAG
HA
FLAG
Lysate
FLAG
HA
B
HA-FASN - +
FLAG-TRIM56 + +
IP:HA
FLAG
HA
Lysate
HA
FLAG
C
HA-FASN - +
IP:HA
TRIM56
HA
Lysate
HA
TRIM56
D
GST-HA + -
GST-HA-FASN - +
FLAG-TRIM56 + +
PD
FLAG
WCL
HA
FLAG
E
GST-HA + -
GST-HA-TRIM56 - +
FLAG-FASN + +
PD
FLAG
WCL
HA
FLAG
F
FASN-TRIM56
KD=1.7 E-8 M
Response (RU)
Time (s)
20 μg/mL
10 μg/mL
5 μg/mL
2.5 μg/mL
1.25 μg/mL
0.625 μg/mL
0.3125 μg/mL
0.15625 μg/mL
0.078125 μg/mL
0.0390625 μg/mL
0.0 μg/mL
G
TRIM56 FL
N
RING
B1
B2
CC
WD40/NHL
C
HA-FASN + + + + + + +
FLAG-TRIM56 - + + + + + +
FL 98-755 1-207 208-755 1-521 522-755
IP:FLAG
HA
Lysate
FLAG
HA
H
FLAG
FLAG-TRIM56
FLAG-TRIM56 (1-521aa)
ns
***
Intra cellular TG (ug/10^6 cells)
PO
I
BSA
PO
FLAG
FLAG -TRIM56
FLAG-TRIM56 (1-521aa)
Nile Red
DAPI
Merge
J
Human hepatocyte cell line
FLAG
FLAG-TRIM56 (1-521aa)
FLAG
FASN
SCD1
ELOVL4
ELOVL6
GPAM
ACTIN
K
FLAG
FLAG-TRIM56 (1-521aa)
ns
Relative mRNA level
SCD1
ELOVL1
ELOVL6
GPAM
DGAT2

753

Fig. 5. TRIM56 interacts with FASN

(A-B) Interaction of FLAG-TRIM56 with HA-FASN in HEK293T cells as demonstrated by IP, n=3.

(C) HA-FASN interacts with endogenous TRIM56 in HEK293T, n=3.

(D-E) GST pulldown assay confirms the interaction between TRIM56 and FASN in HEK293T cells, n=3.

(F) FASN-TRIM56 direct interaction as determined by surface plasmon resonance (SPR) analysis.

(G) Molecular characterization of FASN interaction with different truncated fragments of TRIM56 in HEK293T cells, n=3.

(H) Determination of intracellular TG content in HepG2 transfected with empty vector (FLAG) or FLAG -TRIM56, or FLAG-TRIM56 (1-521aa) fragment in the presence of PO, n=6. One-way ANOVA followed by the Bonferroni post hoc test.

(I) HepG2 were transfected with empty vector or FLAG-TRIM56, or FLAG-TRIM56 (1-521aa) fragment in the presence or absence of PO before Nile Red staining, n=3. Scale bars, 50 μm.

(J) HepG2 were transfected with empty vector (FLAG) or FLAG -TRIM56 (1-521aa) in the presence of PO before whole cell lysate was collected for western blot to determine the expression of proteins related to fatty acid metabolism, n=3.

(K) Expression of indicated genes in HepG2 transfected with empty vector (FLAG) or FLAG-TRIM56 (1-521aa) in the presence of PO, n=5. Two-tailed Student's t-test for *SCD1*, *DGAT2*, Mann-Whitney U test for *ELOVL1*, *ELOVL6*, *GPAM*.

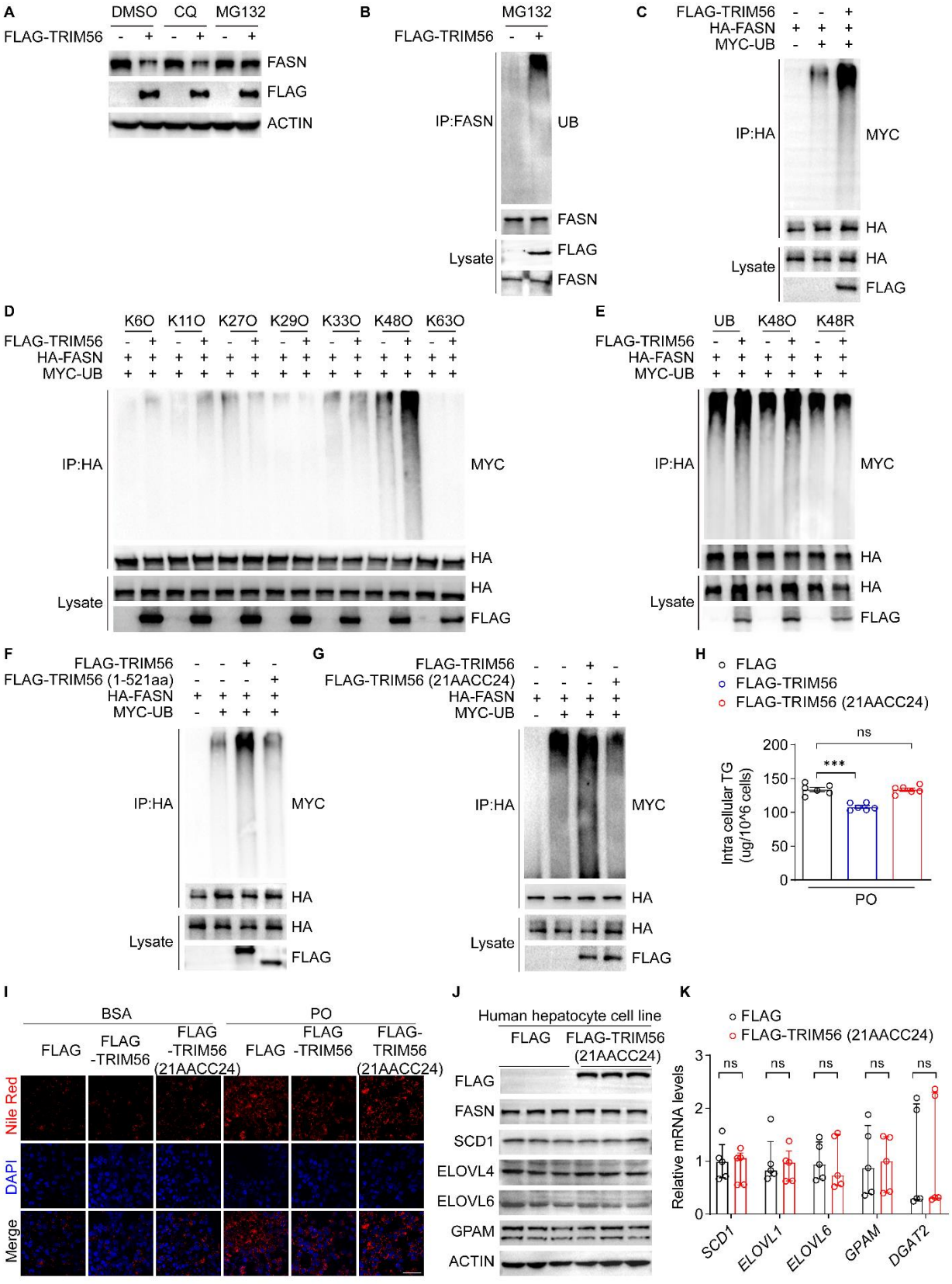
A
DMSO
CQ
MG132
FLAG-TRIM56
FASN
FLAG
ACTIN
B
MG132
FLAG-TRIM56
IP:FASN
UB
FASN
Lysate
FLAG
FASN
C
FLAG-TRIM56
HA-FASN
MYC-UB
IP:HA
MYC
HA
Lysate
HA
FLAG
D
K6O
K11O
K27O
K29O
K33O
K48O
K63O
FLAG-TRIM56
HA-FASN
MYC-UB
IP:HA
MYC
HA
Lysate
HA
FLAG
E
UB
K48O
K48R
FLAG-TRIM56
HA-FASN
MYC-UB
IP:HA
MYC
HA
Lysate
HA
FLAG
F
FLAG-TRIM56
FLAG-TRIM56 (1-521aa)
HA-FASN
MYC-UB
IP:HA
MYC
HA
Lysate
HA
FLAG
G
FLAG-TRIM56
FLAG-TRIM56 (21AACC24)
HA-FASN
MYC-UB
IP:HA
MYC
HA
Lysate
HA
FLAG
H
FLAG
FLAG-TRIM56
FLAG-TRIM56 (21AACC24)
Intra cellular TG (ug/10^6 cells)
200
150
100
50
0
ns
***
PO
I
BSA
PO
FLAG
FLAG -TRIM56
FLAG -TRIM56 (21AACC24)
FLAG
FLAG -TRIM56
FLAG-TRIM56 (21AACC24)
Nile Red
DAPI
Merge
J
Human hepatocyte cell line
FLAG
FLAG-TRIM56 (21AACC24)
FLAG
FASN
SCD1
ELOVL4
ELOVL6
GPAM
ACTIN
K
FLAG
FLAG-TRIM56 (21AACC24)
Relative mRNA levels
3
2
1
0
ns
ns
ns
ns
ns
SCD1
ELOVL1
ELOVL6
GPAM
DGAT2

777

Figure 6. TRIM56 promotes FASN degradation

(A) HepG2 were transfected with empty vector or FLAG-TRIM56 in the presence of absence of DMSO, chloroquine (CQ) or MG132 after PO treatment. Whole cell lysate was collected to determine the protein expression of FASN, n=3.

(B) HEK293T were transfected with empty vector or FLAG-TRIM56 in the presence of MG132. Anti-FASN antibody was used for IP to determine ubiquitinated FASN, n=3.

(C) HEK293T were transfected with HA-FASN in the presence or absence of FLAG-TRIM56 and MYC-ubiquitin. Anti-HA antibody was used for IP to determine ubiquitinated FASN, n=3.

(D) HEK293T were transfected with HA-FASN in the presence or absence of FLAG-TRIM56 and MYC tagged site-specific ubiquitin mutants. Anti-HA antibody was used for IP to determine ubiquitinated FASN, n=3.

(E) HEK293T were transfected with HA-FASN in the presence or absence of FLAG-TRIM56 and Myc tagged active K48-linked ubiquitin (K48O) or inactive K48-linked ubiquitin (K48R) mutants. Anti-HA antibody was used for IP to determine ubiquitinated FASN, n=3.

(F) HEK293T were transfected with HA-FASN in the presence or absence of FLAG-TRIM56 (full length), FLAG-TRIM56 (1-521aa) and MYC-ubiquitin (UB). Anti-HA antibody was used for IP to determine ubiquitinated FASN, n=3.

(G) HEK293T were transfected with HA-FASN in the presence or absence of FLAG-TRIM56, E3 ligase defective mutant FLAG-TRIM56 (21AACC24) and MYC-UB. Anti-HA antibody was used for IP to determine ubiquitinated FASN, n=3.

(H) Intracellular TG content was determined in HepG2 transfected with indicated plasmid vectors in the presence of PO treatment, n=6. One-way ANOVA followed by the Bonferroni post hoc test.

(I) HepG2 were transfected with empty vector (FLAG) or FLAG-TRIM56, or FLAG-TRIM56 mutant (21AACC24) in the presence or absence of PO for 18 h before Nile Red staining, n=3.

(J) HepG2 were transfected with empty vector (FLAG) or FLAG-TRIM56 mutant (21AACC24) in the presence of PO. Whole cell lysate was collected to determine the expression of proteins in lipogenesis pathway, n=3.

(K) Expression of indicated genes in HepG2 transfected with empty vector (FLAG) or FLAG-TRIM56 mutant (21AACC24) in the presence of PO, n=5. two-tailed Student's t-test for SCD1, *GPAM*, Mann-Whitney U test for *ELOVL1*, *ELOVL6*, *DGAT2*.

$*P < 0.05$，$**P<0.01$, and $***P < 0.001$.

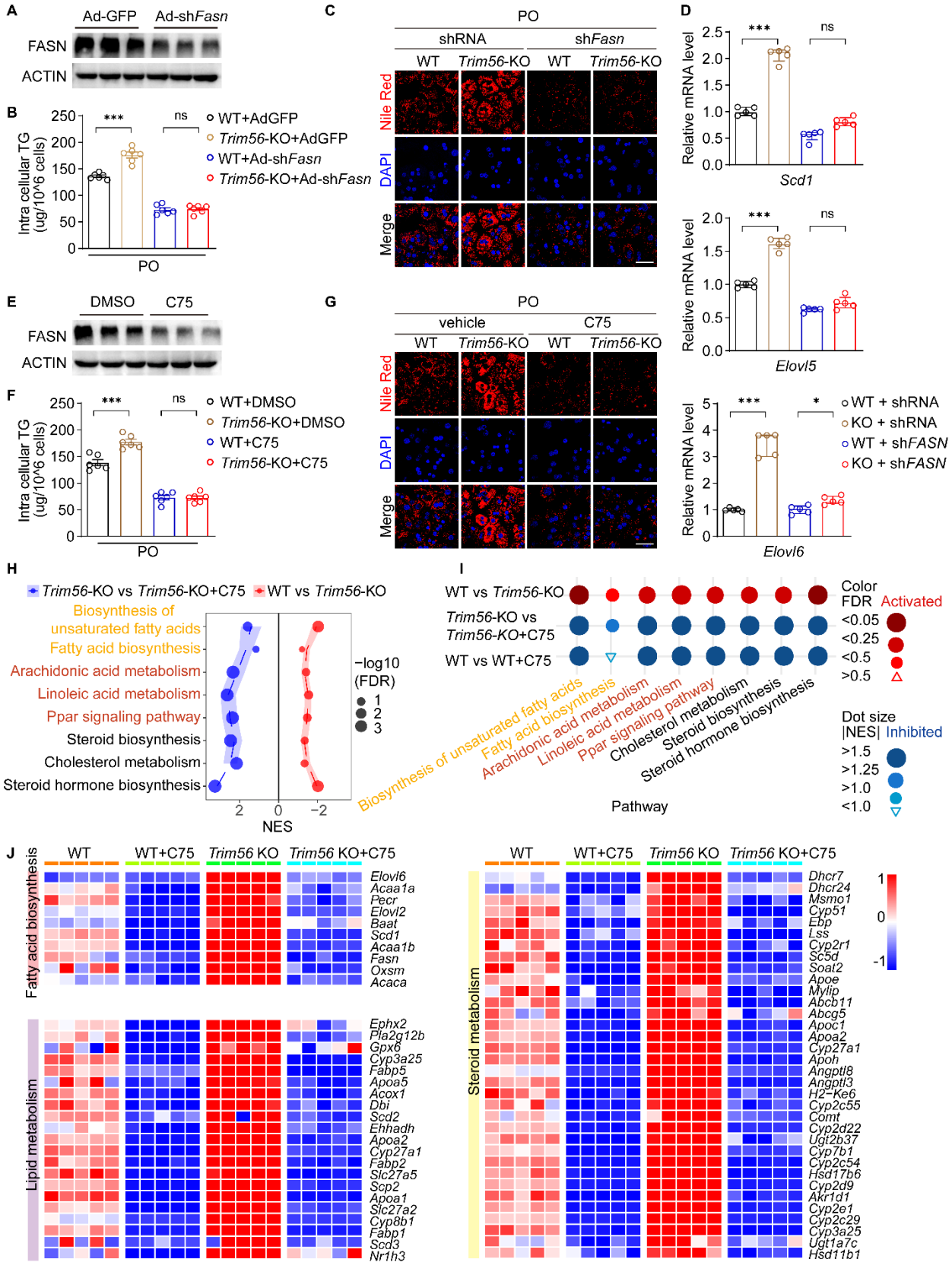
A
Ad-GFP
Ad-shFasn
FASN
ACTIN
B
Intra cellular TG (ug/10^6 cells)
***
ns
WT+AdGFP
Trim56-KO+AdGFP
WT+Ad-shFasn
Trim56-KO+Ad-shFasn
PO
C
PO
shRNA
shFasn
WT
Trim56-KO
Nile Red
DAPI
Merge
D
Relative mRNA level
Scd1
Elovl5
Elovl6
WT + shRNA
KO + shRNA
WT + shFASN
KO + shFASN
E
DMSO
C75
F
WT+DMSO
Trim56-KO+DMSO
WT+C75
Trim56-KO+C75
G
vehicle
H
Trim56-KO vs Trim56-KO+C75
WT vs Trim56-KO
Biosynthesis of unsaturated fatty acids
Fatty acid biosynthesis
Arachidonic acid metabolism
Linoleic acid metabolism
Ppar signaling pathway
Steroid biosynthesis
Cholesterol metabolism
Steroid hormone biosynthesis
−log10 (FDR)
NES
I
WT vs WT+C75
Color
FDR
Activated
Dot size
|NES|
Inhibited
Pathway
J
WT
WT+C75
Trim56 KO
Trim56 KO+C75
Fatty acid biosynthesis
Lipid metabolism
Steroid metabolism
Elovl6
Acaa1a
Pecr
Elovl2
Baat
Scd1
Acaa1b
Fasn
Oxsm
Acaca
Ephx2
Pla2g12b
Gpx6
Cyp3a25
Fabp5
Apoa5
Acox1
Dbi
Scd2
Ehhadh
Apoa2
Cyp27a1
Fabp2
Slc27a5
Scp2
Apoa1
Slc27a2
Cyp8b1
Fabp1
Scd3
Nr1h3
Dhcr7
Dhcr24
Msmo1
Cyp51
Ebp
Lss
Cyp2r1
Sc5d
Soat2
Apoe
Mylip
Abcb11
Abcg5
Apoc1
Apoa2
Cyp27a1
Apoh
Angptl8
Angptl3
H2-Ke6
Cyp2c55
Comt
Cyp2d22
Ugt2b37
Cyp7b1
Cyp2c54
Hsd17b6
Cyp2d9
Akr1d1
Cyp2e1
Cyp2c29
Cyp3a25
Ugt1a7c
Hsd11b1

Fig. 7. FASN inhibition blocks the effect of *Trim56* ablation on lipid accumulation

(A) Silencing efficiency of adenovirus vector encoding shRNA against *Fasn* (Ad-sh*Fasn*) in primary mouse hepatocytes. Hepatocytes were infected with control adenovirus (Ad-GFP) or Ad-sh*Fasn* (MOI=2) for 24 h before whole cell lysate was collected for western blot, n=3.

(B) Primary mouse hepatocytes were isolated from WT and *Trim56*-KO mice. Then, hepatocytes were infected with Ad-GFP or Ad-sh*Fasn* in the presence of PO for 18 h before intracellular TG level was determined, n=6. One-way ANOVA followed by the Bonferroni post hoc test

(C) Nile Red staining of WT and *Trim56*-KO hepatocytes treated as described in B, scale bar 50 μm, n=3.

(D) mRNA expression of *Scd1*, *Elovl5* and *Elovl6* in hepatocytes from indicated groups, n=5. one-way ANOVA followed by the Bonferroni post hoc test for *Elovl5*, Kruskal-Wallis test for *Scd1*, *Elovl6*

(E) Effect of FASN inhibitor C75 on FASN protein expression. Primary mouse hepatocytes were treated with vehicle (0.1%DMSO) or C75 (a pharmacological inhibitor of FASN, 20 μM) for 24 h, n=3.

(F) Primary mouse hepatocytes were isolated from WT and *Trim56*-KO mice. Then, hepatocytes were treated with vehicle or C75 (20 μM) in the presence of PO before intracellular TG analysis, n=6. one-way ANOVA followed by the Bonferroni post hoc test.

(G) Nile Red staining was performed in hepatocytes treated as described in (F), scale bar 50 μm, n=3.

(H) Enriched pathway analysis in WT and *Trim56*-KO hepatocytes treated with vehicle control or C75 (20 μM) in the presence of PO, n=5.

(I) Dot analysis of enriched pathways identified in (H), n=5.

(J) Heatmap analysis reveals the expression profile of genes involved in lipid metabolism, fatty acid biosynthesis and steroid metabolism in WT and *Trim56*-KO hepatocytes treated with vehicle or C75 (20 μM), n=5.

P* < 0.05，*P*<0.01, and ****P* < 0.001.

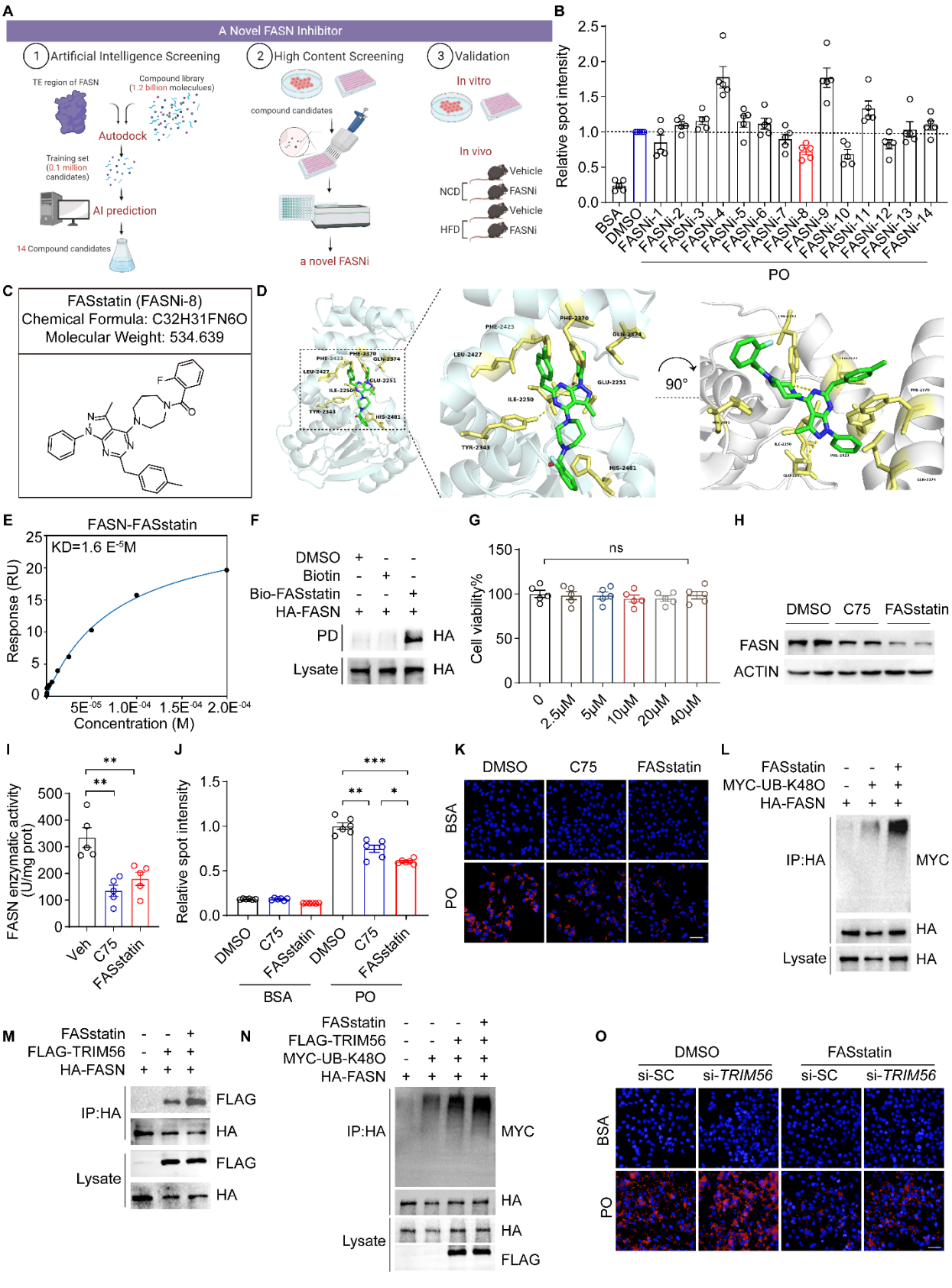
A
A Novel FASN Inhibitor
1 Artificial Intelligence Screening
TE region of FASN
Compound library (1.2 billion molecules)
Autodock
Training set (0.1 million candidates)
AI prediction
14 Compound candidates
2 High Content Screening
compound candidates
a novel FASNi
3 Validation
In vitro
In vivo
Vehicle
NCD
FASNi
Vehicle
HFD
FASNi
B
Relative spot intensity
BSA
DMSO
FASNi-1
FASNi-2
FASNi-3
FASNi-4
FASNi-5
FASNi-6
FASNi-7
FASNi-8
FASNi-9
FASNi-10
FASNi-11
FASNi-12
FASNi-13
FASNi-14
PO
C
FASstatin (FASNi-8)
Chemical Formula: C32H31FN6O
Molecular Weight: 534.639
D
90°
E
FASN-FASstatin
KD=1.6 E-5M
Response (RU)
Concentration (M)
F
DMSO
Biotin
Bio-FASstatin
HA-FASN
PD
HA
Lysate
HA
G
ns
Cell viability%
0
2.5μM
5μM
10μM
20μM
40μM
H
DMSO
C75
FASstatin
FASN
ACTIN
I
FASN enzymatic activity (U/mg prot)
Veh
C75
FASstatin
J
Relative spot intensity
DMSO
C75
FASstatin
DMSO
C75
FASstatin
BSA
PO
K
DMSO
C75
FASstatin
BSA
PO
L
FASstatin
MYC-UB-K48O
HA-FASN
IP:HA
MYC
HA
Lysate
HA
M
FASstatin
FLAG-TRIM56
HA-FASN
IP:HA
FLAG
HA
Lysate
FLAG
HA
N
FASstatin
FLAG-TRIM56
MYC-UB-K48O
HA-FASN
IP:HA
MYC
HA
Lysate
HA
FLAG
O
DMSO
FASstatin
si-SC
si-TRIM56
si-SC
si-TRIM56
BSA
PO

841

Fig. 8. Artificial intelligence (AI)-based compound screening identifies FASstatin as an inhibitor of FASN

(A) High-throughput virtual screening workflow for lead compound identification and pharmacological validation.

(B) Validation of top 14 hit FASN inhibitors (FASNi) by BODIBY staining in PO-challenged human hepatocyte line, n=5. FASNi-8 was named as FASstatin hereafter.

(C) Chemical structure of hit compound FASstatin (FASNi-8).

(D) Molecular docking of FASstatin to the thioesterase domain of FASN.

(E) Interaction of FASN and FASstatin in SPR assay.

(F) Biotin-labeled FASstatin interacts with FASN in streptoavidin-beads pulldown (PD) assay, n=3.

(G) Cell viability assay of HepG2 treated with increasing dose of FASstatin, n=5, one-way ANOVA.

(H) Effects of FASstatin (20 μM) and C75 (20 μM) on FASN protein expression in human hepatocyte cell lines, n=3.

(I) Effect of FASstatin (20 μM) and C75 (20 μM) on FASN enzyme activity, n=5, one-way ANOVA followed by the Bonferroni post hoc test.

(J) Effects of FASstatin (20 μM) and C75 (20 μM) on PO-induced lipid accumulation in Huh7 cells, n=6, one-way ANOVA followed by the Tamhane's T2 analysis.

(K) Representative immunofluorescent images of Nile Red staining of Huh7 cells treated as described in (H), scale bar 50 μm, n=6.

(L) Effect of FASstatin on FASN ubiquitination at Lys 48 in human hepatocyte cell line, n=3.

(M) FASstatin potentiates TRIM56-FASN interaction in HEK293T cells, n=3

(N) Effect of FASstatin on TRIM56-mediated K48-linked ubiquitination of FASN in human hepatocyte cell line, n=3.

(O) Effect of FASstatin on PO-induced lipid accumulation (revealed by Nile Red staining) in TRIM56-depleted hepatocytes. si-SC, scrambled siRNA, si-TRIM56, TRIM56 siRNA, scale bar, 50 μm, n=3.

*$P < 0.05$，**$P<0.01$, and ***$P < 0.001$.

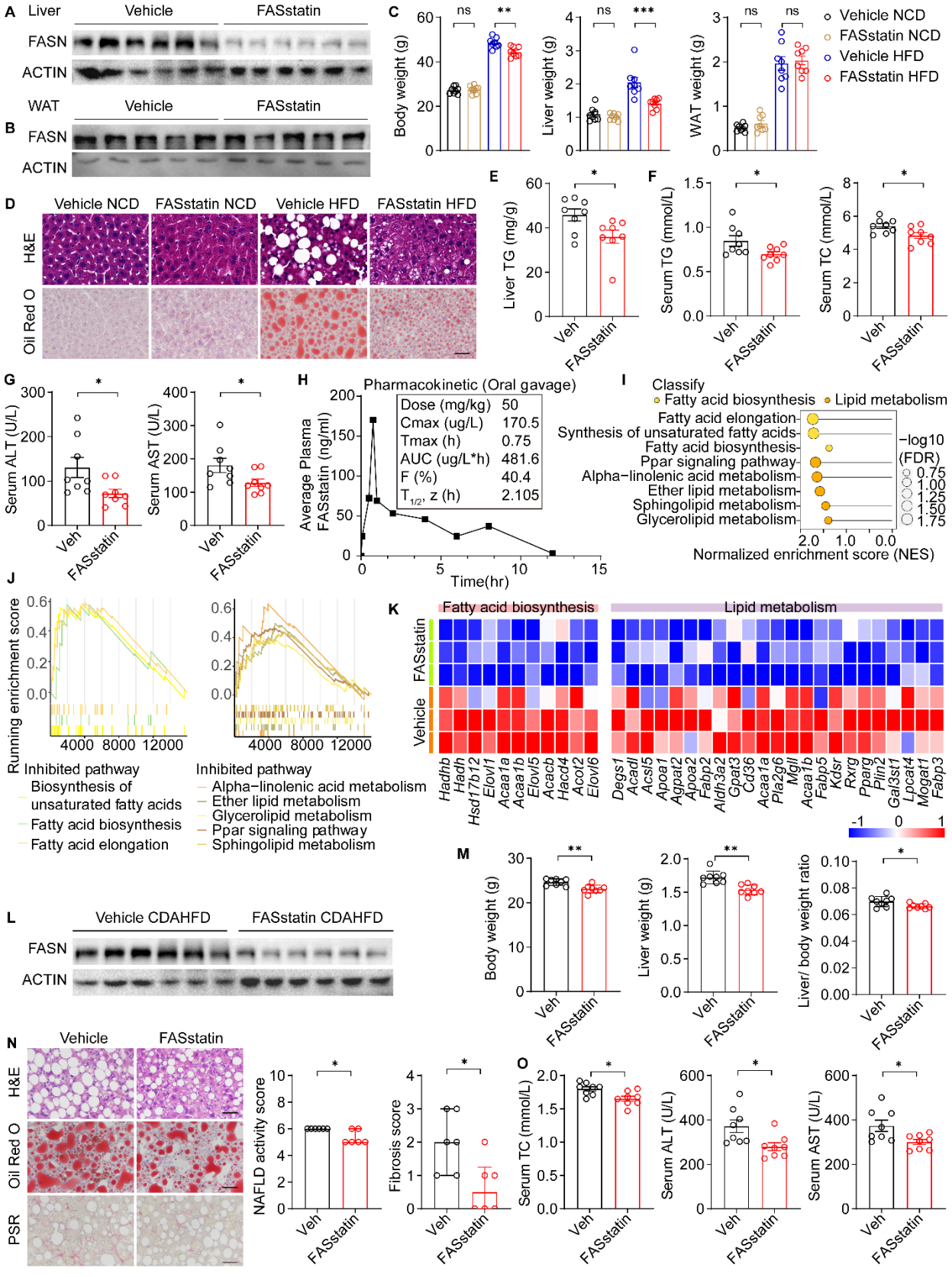
A
Liver
Vehicle
FASstatin
FASN
ACTIN
B
WAT
C
Body weight (g)
Liver weight (g)
WAT weight (g)
ns
**
***
Vehicle NCD
FASstatin NCD
Vehicle HFD
FASstatin HFD
D
H&E
Oil Red O
E
Liver TG (mg/g)
F
Serum TG (mmol/L)
Serum TC (mmol/L)
Veh
FASstatin
G
Serum ALT (U/L)
Serum AST (U/L)
H
Pharmacokinetic (Oral gavage)
Dose (mg/kg) 50
Cmax (ug/L) 170.5
Tmax (h) 0.75
AUC (ug/L*h) 481.6
F (%) 40.4
T1/2, z (h) 2.105
Average Plasma FASstatin (ng/ml)
Time(hr)
I
Classify
Fatty acid biosynthesis
Lipid metabolism
Fatty acid elongation
Synthesis of unsaturated fatty acids
Fatty acid biosynthesis
Ppar signaling pathway
Alpha−linolenic acid metabolism
Ether lipid metabolism
Sphingolipid metabolism
Glycerolipid metabolism
−log10 (FDR)
Normalized enrichment score (NES)
J
Running enrichment score
Inhibited pathway
Biosynthesis of unsaturated fatty acids
Fatty acid biosynthesis
Fatty acid elongation
Alpha−linolenic acid metabolism
Ether lipid metabolism
Glycerolipid metabolism
Ppar signaling pathway
Sphingolipid metabolism
K
Fatty acid biosynthesis
Lipid metabolism
FASstatin
Vehicle
Hadhb Hadh Hsd17b12 Elovl1 Acaa1a Acaa1b Elovl5 Acacb Hacd4 Acot2 Elovl6
Degs1 Acadl Acsl5 Apoa1 Agpat2 Apoa2 Fabp2 Aldh3a2 Gpat3 Cd36 Acaa1a Pla2g6 Mgll Acaa1b Fabp5 Kdsr Rxrg Pparg Plin2 Gal3st1 Lpcat4 Mogat1 Fabp3
M
Body weight (g)
Liver weight (g)
Liver/ body weight ratio
L
Vehicle CDAHFD
FASstatin CDAHFD
FASN
ACTIN
N
Vehicle
FASstatin
H&E
Oil Red O
PSR
NAFLD activity score
Fibrosis score
O
Serum TC (mmol/L)
Serum ALT (U/L)
Serum AST (U/L)

Fig. 9. FASstatin protects against NAFLD and NASH with good safety and oral bioavailability

(A) NAFLD model was established by feeding male C57BL/6J mice with a HFD for 16 weeks. Thereafter, mice were orally administered with vehicle or FASstatin (50 mg/kg/d) for an additional 8 weeks concurrently with HFD feeding. FASN protein expression in livers of NAFLD mice treated with vehicle or FASstatin was examined by western blot analysis, n=6.

(B) Western blot analysis of FASN protein expression in WAT (white adipose tissue) of NAFLD mice treated with vehicle or FASstatin as described in A, n=5.

(C) Body weight, liver weight and WAT weight of mice as described in A, n=8, one-way ANOVA followed by the Bonferroni post hoc test.

(D) Representative images of H&E-stained (top) and Oil Red O–stained (bottom) liver sections from NCD- or HFD-fed mice treated with vehicle or FASstatin for 8 weeks, n=6. Scale bars, 50 μm.

(E) TG content per gram of liver from indicated groups fed with HFD, n=8, two-tailed Student's t-test.

(F) Serum levels of TG and TC levels in vehicle- and FASstatin-treated mice, n=8, two-tailed Student's t-test.

(G) Serum levels of ALT and AST levels in vehicle- and FASstatin-treated mice, n=8, two-tailed Student's t-test.

(H) Pharmacokinetic characterization of FASstatin in the plasma of C57BL/6J mice after single dose of FASstatin administration via oral gavage (50 mg/kg). Plasma was harvested at indicated time and the concentration-time curve was plotted, n=3. Bioavailability factor (F) was calculated.

(I) Pathway enrichment analysis in liver tissues from vehicle or FASstatin-treated mice fed with a HFD, n=3.

(J) GSEA analysis of indicated pathways, n=3.

(K) Heatmap analysis of differentially expressed genes in liver tissues from HFD mice treated with vehicle or FASstatin, n=3.

(L) Effect of FASstatin on FASN protein expression in liver tissues of mice fed with CDAHFD, n=6. Male C57BL/6J mice were fed with CDAHFD for 2 weeks before treatment with vehicle or FASstatin (50 mg/kg/d, i.g.) for an additional 4 weeks.

(M) Effect of FASstatin on liver weight, body weight and liver weight/body weight ratio in mice fed with CDAHFD as described in L, n=8, two-tailed Student's t-test.

(N) Effect of FASstatin on liver pathology (H&E staining), hepatic steatosis (Oil Red O staining) and fibrogenesis (picosirus red staining), NAFLD activity score and fibrosis score, n=6. Scale bars, 50 μm, Mann-Whitney U test.

(O) Effect of FASstatin on serum TC, ALT and AST, n=8, two-tailed Student's t-test.

$*P < 0.05$，$**P<0.01$, and $***P < 0.001$.